A three-dimensional immunofluorescence atlas of the brain of the hackled-orb weaver spider, *Uloborus diversus*.

Gregory Artiushin[1], Abel Corver[2,3,4], Andrew Gordus[1,4]

[1]Department of Biology, Johns Hopkins University, Baltimore, MD

[2]Department of Biology, Lund University, Lund, Sweden

[3]Johns Hopkins Kavli Neuroscience Discovery Institute

[4]Solomon H. Snyder Department of Neuroscience, Johns Hopkins University, Baltimore, MD

Abstract

Spider orb-web building is a captivating, rare example of animal construction, whose neural underpinnings remain undiscovered. An essential step in understanding the basis of this behavior is a foundational mapping of the spider's neuroanatomy, which has thus far been primarily studied using non-web building species. We created a three-dimensional atlas for the hackled orb-weaver, *Uloborus diversus*, based on immunostaining for the presynaptic component, synapsin, in whole-mounted spider synganglia. Aligned to this volume, we examined the expression patterns of neuronal populations representing many of the classical neurotransmitter and neuromodulators, as well as a subset of neuropeptides – detailing immunoreactivity in an unbiased fashion throughout the synganglion, revealing co-expression in known structures, as well as novel neuropils not evident in prior spider works.

This optically-sliced, whole-mount atlas is the first of its kind for spiders, representing a substantive addition to knowledge of brain anatomy and neurotransmitter expression patterns for an orb-weaving species.

Introduction

Brain atlases are essential tools for neuroscience in model organisms – ranging from neuropil annotations (*1*), to neuronal subtype and transcriptional expression pattern atlases (*2*), to ultrastructural connectivity maps (*3*, *4*). In recent years, three-dimensional atlases of major neuropil structures have also been created for non-canonical arthropod study species, including a number of insects (*5*–*7*) and spiders (*8*, *9*).

The hackled orb-weaver spider, *Uloborus diversus* (*10*), is an emerging model system for the study of orb-web building in spiders (*11*, *12*), whose central nervous system has yet to be investigated. To date, the majority of studies of the spider central nervous system have been performed in one, *de facto* model species, *Cupiennius salei (C. salei)*, a cursorial spider which hunts without building webs for prey capture (*13*). While isolated anatomical treatments exist for orb-weavers and other web-based spiders (*9*, *14*–*21*), the preponderance of *C. salei* literature is even starker when considering examinations beyond general neuronal stains, where *C. salei* is essentially the only spider species in which the

expression pattern of more than a single neurotransmitter has been mapped (*14*, *22–32*). Furthermore, the current understanding of spider brain anatomy is almost exclusively based on tissue slice analysis, which can provide exceptional detail, but has the disadvantage of being often limited in completeness by the planes which authors chose to exhibit.

Given that the substantial behavioral adaptation of web-building may be reflected in the presence of necessary brain structures or their proportionality, and certainly in distinct underlying neuronal circuitry, an important step in understanding the basis of this behavior is to have a foundational architecture of a nervous system which generates it. We created a three-dimensional immunofluorescence atlas of major neurotransmitter and neuromodulator populations for *U. diversus*, using whole-mounted synganglia. Using immunostaining against the presynaptic marker, synapsin, we assembled a standard, full volume of *U. diversus* synganglion onto which specific neurosignaling molecule expression patterns were aligned. These include markers for classical neurotransmitters (GABA, acetylcholine), neuromodulators (dopamine, serotonin, octopamine/tyramine) and several neuropeptides (AllatostatinA, Proctolin, CCAP, FMRFamide). These volumes provide comprehensive and comparable detail throughout the synganglion, in both undifferentiated and established regions – such as the arcuate body, whose layers become distinguishable through the use of neurosignaling molecule co-stains. We further identify several previously undescribed neuropils in the supraesophageal ganglion, and the neuronal subtype populations whose specific expression demarcates them.

Results

The central nervous system of spiders is distinctive among arthropods for its compressed nature. Residing within the prosoma, the synganglion is a fusion of two major ganglia, named in reference to the esophageal passage running between them – the subesophageal ganglion, comprised primarily of motor and sensory interneurons and comparable to the ventral nerve cord in insects, and the supraesophageal ganglion, considered the brain proper, containing the higher-order integration centers (Fig. 1a).

Consistent with general arthropod nervous system morphology, the neuronal somata are arranged superficially around the synganglion (Fig. 1b,c), while all the internal tissue is neuropil. An averaged volume of anti-synapsin immunostaining (for neuropil) and DAPI stain (for nuclei), reveals that a substantial proportion of somata are found on the ventral side of the subesophageal ganglion, with some nuclei found laterally, but little to any on the dorsal surface of the subesophageal ganglion. A clear patch is also present on the posterior aspect adjoining the opisthosomal neuromere. Nuclei are found completely throughout the ventral-dorsal plane of the anterior side of the synganglion, with populations also seen on the lateral sides (Fig. 1b,d).

In the supraesophageal ganglion as well, nuclei are not present on the posterior side, except for at the dorsal-most end, where a cap of DAPI-positive staining enveils the posterior, anterior, lateral, and dorsal aspects of the supraesophageal ganglion, beginning approximately at the level of arcuate body (Fig 1b,c).

Within the subesophageal ganglion there are a limited number of conspicuous neuropils, which are evident from the exterior, and have been previously described in other species (*8*, *9*, *13*). Most ventrally,

a bulk of the subesophageal ganglion is comprised of four leg ganglia (or neuromeres) per hemiganglia, corresponding to the eight legs of the spider (Fig. 2a-e).

Supplying these neuropils, as well as others and founding the longitudinal connections between the major ganglia, are a series of major nested fiber tracts, having a stacked organization in both the medio-lateral and ventro-dorsal planes. A chiasm structure is visible at the midline (Fig. 2c,d) with the synaptically-negative circular openings assumed to be tracheal passageways. Throughout these same planes, the pedipalpal neuropil appears anteriorly (Fig. 2b-e).

Further dorsally (Fig. 2f,g), the tract pattern takes on a ladder appearance, which correspond to an arcade of finer commissures, not visible in this representation. These commissures connect all major neuropils of the subesophageal ganglion. The courses of these tracts are most comprehensible when followed by studying individual neurosignaling molecule stains, as exemplified by anti-tyrosine hydroxylase immunofluorescence, discussed below.

The opisthosomal neuromere, supplying the hind compartment of the spider body, starts to emerge (Fig. 2f, g), and will reach its full width in a shared plane with the esophageal passage (Fig. 2h,i) before diminishing more dorsally after the esophageal passage closes (Fig. 2j,k). Within the opisthosomal neuropil, a ladder-like appearance of medio-laterally running tracts can also be appreciated (Fig. 2g-i). Posteriorly travelling tracts also diverge laterally to follow the circumference of the opisthosomal neuropil (Fig. 2i).

At the level of the esophageal passage, an anterior-lateral neuropil begins to form, wrapping medially to form the cheliceral neuropil (Fig. 2g-i), as medially the esophageal passage begins to close. The esophageal passage is bridged at the anterior side by a region named the stomodeal bridge (Fig. 2j) (*8*). A bridge structure also exists at the posterior end, where additional undifferentiated synaptic density is flanking. Within this plane (Fig. 2j), the protocerebral tract is essentially parallel to the ventro-dorsal axis, and appears as twin, dense nodes rising in the central burgeoning supraesophageal ganglion.

Subesophageal ganglion features and expression patterns:

Explorations of neurosignaling population innervation in the subesophageal ganglion have generally been less detailed than within the supraesophageal ganglion. Certain neuropeptides were either only briefly shown to be immunoreactive (such as AllatostatinA (*8*)) or not presented on in the subesophageal ganglion (e.g. CCAP (*28*)). We find that all neuropeptidergic antisera, as well as the others, examined in this study have robust expression throughout the subesophageal ganglion. One observation which does not appear to be previously noted is that there is a roughly equal anterior/posterior division in the leg neuromeres. Whereas some immunostains reveal equal innervation of the halves (α-TH), others show divergent patterns (α-TDC2), or predominant expression in only one compartment (α-AstA). Based on select examples where the origin of innervation is discernable, the posterior and anterior compartments of the leg neuropils may be supplied by neurites from different tracts within the interior of the subesophageal ganglion.

The opisthosomal neuropil is a section of the subesophageal ganglion which has received relatively less attention. The preeminent reference for major tracts within the spider synganglion is the treatment in *C. salei* (*13*), but despite a detailed annotation throughout the synganglion, the trajectories within the

opisthosomal ganglion were not diagrammed. A more recent expansion of this anatomical knowledge to further cursorial as well as web-based species of spiders (*9*) likewise did not comment on the opisthosomal neuropil. A depiction from Hanström (*33*), shows that longitudinal tracts run parallel to the midline, as well as more laterally, and that there are crossing branches between them, forming a ladder-like architecture. This bears a resemblance to the pattern revealed by specific antisera in *U. diversus*, confirming the central tracts, perimeter defining tracts, as well as crossing fibers within the opisthosomal ganglion – though whether they cross completely from midline to periphery was not apparent. In certain cases we observed a ladder structure as well as a ring-like central structure with neurites projecting like spokes. Immunoreactivity within the opisthosomal ganglion was variable between target neurosignaling molecules. One additional subesophageal feature previously identified in *C. salei* is the Blumenthal neuropil (*34*), which is innervated by afferents from the thermoreceptive and hygroreceptive tarsal organ. Although we also see a paired, synapsin-density close to the midline in the approximate anterio-ventral subesophageal location as described for *C. salei*, we cannot be confident that this is the same structure – a question which will benefit from tracing techniques.

Acetylcholine:

In order to visualize acetylcholinergic populations and their expression patterns, we employed antisera for choline acetyltransferase (ChAT). To our knowledge, the only previous study of cholinergic neurons in the spider CNS was done in the wandering spider, *Cupiennius salei* (*30*).

Beginning ventrally, numerous ChAT+ somata are seen in the dense field of neurons located medially from the leg neuromeres along the midline of the hemiganglia (Fig. S1a). Cholinergic neurons are also present between leg neuromeres in the anterior-posterior direction, and for both cases, there is a diversity of both size and staining intensity. The interspersed presence of more intensely ChAT-immunoreactive neurons within the subesophageal ganglion was also observed in *C. salei* (*30*). At approximately the level of the pedipalp ganglia (Fig. S1b, arrows) there are 3-4 relatively smaller, strongly immunoreactive somata.

GABA:

GABAergic neurons can be identified with antisera to γ-aminobutyric acid (GAD) and have been studied in the CNS in *C. salei* (*26*, *29*) as well as the barn spider, *Araneus cavaticus* (*15*) and *Achaearanea tepidariorum* (also known as *Parasteatoda tepidariorum* (*17*). GABAergic neurons are the most populous subtype that we have visualized in *U. diversus*, with a large portion of these cells residing on the ventral surface in the subesophageal ganglion (Fig. S2a-b), with presence posteriorly as well, ventral to the opisthosomal neuropil (Fig. S2c). While used coincidentally with other successful antibodies by our standard preparation, GAD antisera unfortunately exhibited poor signal penetration in the interior of the tissue, limiting our analysis to the presence of GAD+ somata, as well as a number of neuropil features which happened to be closer to the surface of the tissue, such as the opisthosomal neuropil (Fig. S2d).

Dopamine:

In contrast to all other neurosignaling molecules, dopaminergic innervation of the spider brain has not been investigated in *C. salei*, but rather in the wolf spider, *Hogna lenta*, and the jumping spider, *Phidippus regius*, where it was interrogated using antisera to core synthesizing enzyme, tyrosine hydroxylase (*35*).

We found this antibody to be effective in *U. diversus*, staining both cell bodies and projections with enough clarity to follow the innervation patterns of many individual dopaminergic neurons. Associated with each of the leg neuromeres are 7-8 TH+ neurons (Fig. S3a). The positioning of these is somewhat variable, but it appears that they form two subgroups – a cluster of 5-6 smaller neurons (Fig. S3a – arrowheads), typically with a couple being less intensely immunoreactive to TH, and the remaining 1-2 larger neurons which are spaced further from the rest (Fig. S3a – arrows). Dopaminergic projections clearly trace each of the 4 leg neuromere commissures, as well as two anterior commissures (Fig. S3e). The smaller subset appears to give rise to the leg neuromere commissures, as well as supplying some innervation within the neuromere. The projections of the more populous cluster are more difficult to follow, but presumably contribute to the neuromere pattern. Each leg neuromere is evenly filled by a mesh network of dopaminergic varicosities (Fig. S3b).

Medio-ventral to the pedipalp neuromere are a cluster of 2-3 TH+ neurons per hemiganglia in the anterior field of somata (Fig. S3c, d - arrows). The projections of these neurons can be traced through the pedipalp and cheliceral commissures, suggesting that they are supplying both of the respective neuropils. The posterior of these commissures (pedipalp) is subdivided into two tracts which mingle at the midline. Posterior to these neurons is an area of denser immunoreactivity continuous with the strongly labelled anterior-most arching commissure of the dorsal-tract (as referred to by Auletta et al (*35*), for the same antibody).

Serotonin:

To visualize serotonergic populations we used an antibody raised directly against serotonin. The patterning of serotonergic innervation has been studied throughout the synganglion in *C. salei* – although only a literal description has been accessible to us (*22*) – and briefly shown for the arcuate body in the wolf spider, *Pardosa* (*36*). Matching what has been reported for *C. salei* (*22*), a cluster of ~5 serotonin-positive cells are evident adjacent to each leg neuromere (Fig. S4a).

Most notably in the neuromeres of Legs I (anterior), the serotonergic innervation in the limb neuroarchitecture appears to be supplied in two roughly equal halves, filling the periphery and leaving an area dark of immunoreactivity within (Fig. S4b – brace). The anterior half of the innervation appears to be supplied from the medial branch of the "dorsal-most tract" (as referenced by Auletta et al. (*35*)). Several 5-HT+ neurons are seen ventral to the pedipalp neuropil (Fig. S4c – arrows), which has serotonergic immunoreactivity on the medial portions flanking the midline. Ventral to the opisthosomal neuromere are clusters of serotonergic somata which project into a robust tract travelling medially (Fig. S4d – arrows).

Octopamine/Tyramine:

The antisera which we screened for individual octopaminergic and tyraminergic populations were not found to be effective. Tyrosine decarboxylase 2 (TDC2) is an enzyme the catalyzes the conversion of tyrosine to tyramine, which is subsequently necessary for octopamine metabolism, meaning that TDC2 is present in both neuronal subtypes in invertebrates. We found a *Drosophila melanogaster* antibody to TDC2 to be effective in *U. diversus.*

Given that TDC2-immunoreacitivty should include both octopaminergic and tyraminergic neurons, we might expect that potentially more positive somata would be seen in *U. diversus* than in *C. salei*, where octopamine was stained for directly (*24*), assuming the relative population sizes in the species are equal. Instead in the subesophageal ganglion we find a cluster of 5-6 TDC2+ somata per leg neuromere (Fig. S5a), which is fewer than for C. salei (*24*). Unlike the uniform mesh-like innervation of each leg neuromere produced by dopaminergic neurons, or the more or less symmetrical pattern for serotonin, the pattern in TDC2 staining is notably different. The anterior side of each neuromere contains a patch of continuous, diffuse, and more lightly stained immunoreactivity, while on each posterior side there is a swath of brightly reactive, sparse puncta (Fig S5b).

All subesophageal ganglion tracts and commissures which were revealed by fine dopaminergic projections are likewise labelled with TDC2-immunoreactivity. We also observed somata ventral to the opisthosomal neuromere (Fig. S5c – arrows), but did not see any such gargantuan cell bodies as seen in this vicinity in *C. salei* (*24*). There is substantial TDC2-immunoreactivity in the pedipalpal (Fig. S5c) and cheliceral neuromeres (Fig. S5d).

TDC2-immunoreactivity displays an intricate pattern within the opisthosomal neuromere. At the ventral anterior end two triangular formations of puncta (Fig. S5d – brace) abut the input of a string of varicosities on each lateral side, which then becomes heavier and continues to outline the boundary of the opisthosomal neuromere (Fig. S5d – arrow). An approximately mirrored pair of immunoreactive triangles are found with their apex pointing posteriorly, at the posterior end of this neuromere. Within the interior of the opisthosomal neuromere, fibers resembling spokes emanate to a ring-like midline where there is a small chiasm, and a thicker bridge structure joining lateral segments which travel in the anterior-posterior direction.

AstA:

The earlier work in *C. salei* (*28*) did not comment on AstA-immunoreactivity outside of the dorsal supraesophageal ganglion, but an image from the jumping spider, *Marpissa muscosa*, confirms that AstA-immunoreactive expression is present throughout the synganglion (*8*). In the far ventral portion of the subesophageal ganglion where there is a complete covering of somata, there are paired clusters of 3 – 4 large AstA+ somata located on the posterior side (Fig. S6a – arrow). In a similar plane, there are two smaller somata located along the midline (Fig. S6a). AstA-immunoreactivity has a distinctive pattern within the leg neuromeres, showing robust varicosities but only the posterior portion of neuromere (Fig. S6b,c). This innervation appears to be supplied from the lateral branches of the centro-lateral tract.

Similar to what has been described for *M. muscosa* as the stomodeal bridge, the area adjacent to the esophagus on the anterior side of the subesophageal ganglion is prominently immunoreactive to allatostatin (Fig. S6d – brace), although the actual bridge which crosses the midline is more modest than

236 in other stains, having only a few neurites, and thin representation in the posterior commissure (Fig. S6e
237 – arrow). Faint somata are also seen closely anterior to this region.
238

239 *Proctolin*:

240 Proctolin expression patterns were previously explored in *C. salei* both throughout the CNS (*26*, *32*), as
241 well as in a focused manner in the protocerebrum, as a means to reveal arcuate body layering (Loesel et
242 al., 2011). Beginning in the subesophageal ganglion, proctolin-immunoreactive somata were found in
243 clusters of multiple somata along each neuromere ((*37*) citing Duncker et al., 1992), as well as many
244 other weakly labelled Proc+ cells (*32*). Curiously, in *U. diversus* we see a single bright Proc+ soma
245 associated with each of the 8 leg neuromeres in the subesophageal ganglion (Fig. S7a). These neurons
246 are found approximately at the same area as clusters for other populations, such as the aforementioned
247 monoamines. They are generally posterior and medial to the bulk of the respective leg neuromere.
248 Smaller and faintly immunoreactive Proc+ neurons are also seen in the vicinity and it is possible that our
249 sensitivity to weakly-labelled somata is lesser than in stained slices.
250
251 Medial to the emerging pedipalp neuropils are 2-3 Proctolin+ somata projecting a neurite into the
252 strongly staining anterior zone, also highlighted by serotonergic innervation (Fig. S7b – arrow). Likewise
253 in this plane, densely labeled somata are present in the field ventral to the opisthosomal neuromere (Fig.
254 S7b – arrowhead). A circular form of saturated proctolin-immunoreactivity is seen at the posterior end of
255 an oval shaped synapsin-density (Fig. S7c – arrow), suggesting that it is a subset of a major tract bundle.
256 In dorsal planes this immonreactivity morphs into lateral moving strands of varicosities becoming
257 difficult to trace. Such an appearance is not found in the other neurosignaling molecule stains, even
258 those with profound subesophageal expression.
259
260 The fine neurites projecting to the center of the opisthosomal neuropil as seen for TDC2 are also
261 apparent for proctolin-immunoreactivity (Fig. S7d).
262

263 *CCAP*:

264 Despite its name alluding to function in the heart, CCAP has considerable immunoreactivity throughout
265 the sub- and supraesophageal ganglia in *U. diversus*. The one prior investigation of CCAP in *C. salei*
266 presented CCAP expression patterns only for the brain (*28*). In our volumes, a cluster of ~5 intensely
267 immunoreactive neurons is seen around the Leg IV neuromere (Fig. S8a), and positive somata are also
268 associated with the opisthosomal neuromere (Fig. S8c – arrow). CCAP-immunoreactive neurons are
269 present in a more dispersed fashion within the ventral subesophageal ganglion (Fig. S8b).
270 Immunoreactivity within the leg neuropils is predominantly in the posterior halves, where sparse puncta
271 are evenly distributed (Fig. S8b).
272

273 *FMRFamide*:

274 At the ventral end of the synganglion, FMRFamide+ neurons are numerous and dispersed throughout the
275 width of the ventral field of somata (Fig. S9a). Unlike other neuropeptides and monoamines, these
276 immunoreactive somata cannot be readily attributed to clusters corresponding to individual
277 neuromeres. A concentration of FMRFamide neurons are present in the somata field ventral to the
278 opisthosomal neuromere (Fig. S9b – arrows), which was also found for *C. salei* (*30*). Ample FMRFamide

signal is seen within the opisthosomal neuromere (Fig. S9c-e). FMRFamide+ neurons are also prevalent around the cheliceral neuromeres in the area of the stomodeal bridge (Fig. S9d – arrows).

Supraesophageal ganglion features:

Within the supraesophageal ganglion reside a number of dense neuropil regions which are discernible from their surroundings. These include major recognizable structures such as the mushroom bodies (Fig. 2m-o) and arcuate body (Fig. 2q-t), as well as some previously undescribed structures, made evident by the present image volumes.

The protocerebral tract can be followed further dorsally (Fig. 2j-l). The protocerebral tract dissipates, and the protocerebral commissure (PCC) appears centrally (Fig. 2l). In this plane, the brightest lateral structures are the hafts, the ventral-most reaches of the mushroom bodies. The neuropil directly anterior to the PCC, paired and adjacent to the midline, forms a distinct landmark, which we refer to it as the 'hagstone' neuropil, given its pendular and pierced form (Fig. 2m). Continuing dorsally (Fig. 2n), the bulk of the mushroom bodies is present, the hagstone neuropil persists, and a faintly arching, umbrella-like density is visible at the posterior side of the supraesophageal ganglion. The mushroom body bridge and head is found dorsally (Fig. 2o), and centrally, an ovoid neuropil coalesces (Fig. 2p-r), which has not been apparent in previous anatomical investigations (tonsillar neuropil, Fig. 2q). The arcuate body lobes are present on the posterior side of the dorsal supraesophageal ganglion (Fig. 2 q-t), while anterio-laterally a previously uncharacterized banded neuropil structure is visible (protocerebral bridge (PCB) neuropil, Fig. 2S-t).

Mushroom bodies

The mushroom bodies (MBs) (or corpora pendunculata) are a paired neuropil structure whose size, shape and mere presence are substantially variable across not only chelicerates, but arthropods in general. Their fundamental morphological attributes are a stalk and head region reflecting their namesake structure, and their mirrored distribution in the hemiganglia. Best characterized in insect model species, and while sharing in anatomical and molecular characteristics (*38*), the evolutionary relationship of insect MBs to those of chelicerates and other arthropods, and particularly spiders, has been a continuing debate (*9*, *38–40*).

The mushroom bodies of *U. diversus* (Fig. 3a,b) tend to show the most robust synpasin-immunoreactivity of all structures in the supraesophageal ganglion (Fig. 3c, maximum intensity projection), indicating a great degree of synaptic density. While web-building species have been reported to have simplified (*9*) or even entirely absent mushroom bodies (*9*, *20*, *33*), these structures are present in *U. diversus* and retain the complete form seen in more visually-reliant species (*8*, *9*), even if they are smaller relative to the supraesophageal ganglion as a whole (Fig. 3a,b,c).

U. diversus MBs display a haft, body and head region, with the two hemiganglion pairs connected by a bridge (Fig. 3a-c). Synapsin-immunoreactivity is modest within the bridge region, whose true thickness is better visualized with staining for βTubulin3 (Fig. 3d). Despite the strong synapsin-immunoreactivity in the MBs, we surprisingly did not see co-expression with most of our specific neurosignaling molecule antibodies. This pattern is also reflected in the extant spider literature, with a single study showing immunoreactivity in the mushroom bodies of *C. salei* for anti-GAD and anti-proctolin staining (*26*). In our

320 hands, only anti-AllatostatinA staining showed co-immunoreactivity throughout the mushroom body
321 (Fig. 3e). Although difficult to trace the source far, it appears the hafts are innervated from the posterior
322 side (Fig. 3f). By βTubulin3-immunoreactivity, we observe two tracts which straddle the MB hafts as they
323 descend from the dorsal somata layer (Fig. 3g). Finer neurites are not distinguishable in the βTub3-
324 immunoreactivity, but it seems plausible that the AstA+ neurites entering the MB hafts might stem from
325 the medial of these two tracts.

326 Babu and Barth (1984) described the protocerebro-dorsal tract as providing input to the hafts of the
327 mushroom bodies. The connection of this tract to the MB hafts is not apparent by our synapsin stains in
328 *U. diversus*, which was likewise the case with silver staining for *P. amentata*, *M. muscosa*, *A. bruennichi*,
329 and *P. tepidariorum* (*9*).

330 The antero-dorsal input to the MB heads, representing the secondary eye pathway (*39*), is much more
331 conspicuous and has received considerable treatment within the literature. The mushroom body heads
332 are sometimes referred as the third-order visual neuropil in this pathway, with the ample parallel fibers
333 which give this structure its shape arising from globuli cells which cap the mushroom body head.

334 The globuli cells are not distinguishable from the surrounding nuclei by DAPI signal, but can potentially
335 be discerned through specific neurosignaling molecule immunostains. We find the cluster of cells closely
336 associated with the MB heads are revealed by ChAT-immunoreactivity, and to a lesser extent by GAD-
337 immunoreactivity, suggesting they represent cholinergic and GABAergic populations, respectively (see
338 Acetylcholine and GABA subsections, below). Globuli cells in *C. salei* have previously been shown to be
339 ChAT+ (*30*). By βTubulin3 staining, we also observed a trident of tracts feeding into the dorsal aspect of
340 the mushroom body head (Fig. 3g).

341

342 **Visual System**

343 *U. diversus,* like many orb-weavers, builds its web in the night and can do so in essentially complete
344 darkness in laboratory conditions, suggesting that vision is expendable to much of the spider's
345 behavioral repertoire (*41*). Web-building spiders are considered to have poorer vision than spiders
346 which depend on sight to capture prey, which is reflected in their diminished optic neuropils and tract
347 pathways (*9*, *21*).

348 Relative to cursorial species (*8*, *9*, *13*), in *U. diversus* the anterior extensions of the protocerebrum
349 containing the first and second-order optic neuropils are considerably thinner and not as extensively
350 fused with the continuous neuropil of the supraesophageal ganglion, and are prone to separating during
351 dissection. Consequently, neither the primary or secondary visual pathway neuropils appear reliably
352 enough in the anti-synapsin volumes to be apparent in the averaged standard brain representation, but
353 nevertheless these structures are exhibited in various individual preparations. The optic neuropils in *U.*
354 *diversus* tended to show weaker synapins-immuoreactivity, but were clearly seen with antisera to HRP
355 (Fig. 4a).

356 As in other species, the secondary pathway is larger (Fig. 4b), lifting away anteriodorsally to the zone of
357 the MB heads. This continuity can be inferred from the sliced three-dimensional maximum intensity
358 projection of synapsin (Fig. 4b). The primary pathway is diminutive in *U. diversus*, and emerges as a
359 bulbous shape at the dorsal-most end of the brain through a field of somata (Fig. 4a).

Previous reports have used GABA (*26*), histamine (*23*), dopamine (*35*), CCAP (*28*), and FMRFamide (*26*) to reveal the successive neuropils of the visual pathways. As noted above, the only features within the optic pathway for which we observed neurosignaling molecule immunoreactivity were the globuli cells with GAD and ChAT staining. It is possible that targets for which we could not acquire an effective antisera, such as histamine, could be revelatory of the optic lamellae and other visual pathway structures, as they have been for *C. salei* (*14*, *23*). Specific compartments of the pathways, such as the medulla or lamellae could not be discerned with any preparation.

Arcuate body:

The arcuate body is a prominent neuropil structure found in all spider species whose central nervous system anatomy has been examined closely to date. Residing in the dorso-posterior aspect of the supra-esophageal ganglion, this solitary crescent-shaped structure has been recognized as having at least two broad divisions, the ventral and dorsal lobes (*8*, *28*, *33*).

Additional layers have been noted by synapsin staining in the dorsal arcuate body (*8*). The precise number of layers varies within the literature, and it is unclear to what extent authors distinguish between the gross lobes of the AB, and sublayers which may be found within. This is also complicated by the fact that slices are not always made in a consistent orientation. In absence of a whole-mounted example or a seamless stack of slices, an oblique slice may over- or underestimate the size of a layer, depending on the angle taken. Additionally, the degree of layering may also reflect a true difference between species, independent of methodology.

In *U. diversus*, at the grossest level, we likewise observe two lobes of the arcuate body, which we will refer to as the ventral (ABv) and dorsal (ABd) (Fig. 5a,b). Though largely coincident in the dorso-ventral axis, the ventral arcuate body somewhat envelopes the dorsal arcuate lobe, hence appearing first from the ventral direction and lingering posteriorly on the dorsal side, with only a smaller part of the dorsal arcuate body protruding independently beyond the ABv at the dorsal end (Fig. 5b).

Each lobe (ABv and ABd) can be further subdivided into two sub-lobes or layers – a posterior (posABv and posABd) and anterior (antABv and antABd) section, making a total of four units (Fig. 5c). The sublayers of the arcuate body lobes are distinguishable by immunostaining for specific neuronal subpopulations which differentially innervate the layers (Fig. 5d, Fig. 6). By examining these expression patterns, another tier of complexity can be appreciated, as each of these sublayers (posABv, antAbv, posABd, antABd) can be further subdivided into 2 or even 3 aspects, depending on the antisera used.

There is a diversity of layering patterns (Fig. 6), but some basic motifs emerge. Innervation can be partial, as in filling a single sublayer (anterior or posterior) of a lobe, or complete throughout the lobe, taking on a saturated appearance, a meshwork of neurites, or a sparse field of puncta. The space between marked sublayers may at times have finer neurite connections which have been described as palisade-like (*28*). Most commonly at the dorsal end of the ventral arcuate body (ABv), heavy garland-like varicosities may form, in certain examples (α-Proctolin, α-TDC2, α-FMRFamide, Fig. 6) appearing as disjointed units, suggestive of an undergirding column. More prevalently in the dorsal arcuate, a robust networking of thicker immunoreactive fibers weave between roughly trapezoidal signal-negative areas

402 (α-5-HT, α-TDC2, Fig. 6), resembling a flagstone pathway. Detailed descriptions of arcuate body layer
403 projection patterns (Fig. 6) and comparisons to other spider species are found below in the respective
404 subsections for each neurosignaling molecule.

405 The innervation pattern of a given neuronal subpopulation in a layer of the arcuate body is not a general
406 delineation of the structure of that layer, as different transmitter populations can display distinct
407 expression patterns within the same layer. An example is the dorsal arcuate body (ABd), where TDC2-
408 immunoreactivity shows a prominent columnar, flagstone innervation, while proctolin has a sparse field
409 of fine puncta in the same layer (Fig. 5f).

410 Posterior to the arcuate body is crest of somata which has been previously referred to as the posterior
411 cell layer (PCL) (*30*). Neurons of the PCL send their projections anteriorly through the ventral arcuate
412 layers, as revealed by immunostaining for βTubulin3 in conjunction with synapsin (Fig. 5e). The fibers
413 successively run medially as one progresses further dorsally in the arcuate lobes, with certain tracts
414 being thicker than others. Hill noted the presence of tracts running through the arcuate body to join the
415 PCDt in jumping spider, *P. johnsoni* (*42*).

416 *Acetylcholine*:

417 In the arcuate body, cholinergic signal is predominantly found in the ventral arcuate body lobe (Fig. 6 -
418 α-ChAT, ventral, Fig. S1 h,i). Within the ventral side of this lobe, cholinergic signal forms fine puncta
419 which completely fill the anterior sub-layer of this lobe. Toward the dorsal end of this lobe, the punctate
420 immunoreactivity forms heavier beaded varicosities. Midway there are faint column-like expression
421 patterns joining from a thin layer within the posterior ventral AB (pABv). A single layer is sparsely
422 innervated on the anterior side of the dorsal lobe (Fig. 6) (Fig. 6 - α-ChAT, dorsal). Cholinergic
423 innervation within the layers of the arcuate body has yet to be described for any other spider species.

424 *GABA:*

425 In the ventral lobe of the arcuate body are several layers of faint GAD-immunoreactivity (Fig. S2g, Fig. 6 -
426 α-GAD). At the edge of the posterior layer, GAD+ somata of the adjacent posterior cell layer are seen,
427 anterior to which there is wider layer fine signal (Fig. 6 - α-GAD, ventral). Moving anteriorly, this is
428 followed by a very thin layer of puncta which may be connected through minute projections to the next
429 layer which is as thick as the first. The anterior-most layer of the ventral lobe appears empty of
430 immunoreactivity. Apart from a haze which is difficult to disentangle from bleedthrough or background,
431 the same can be said of the dorsal arcuate body lobe. However, in the dorsal arcuate body lobe we see a
432 clear illustration of how neurites stemming from the somata of the posterior cell layer extend through
433 the arcuate body layers (Fig. 6 - α-GAD, ventral). The pattern in *C. salei* (*26*, *29*) is similar for the first
434 layers beginning from the posterior side, but diverges at the anterior-most arcuate body section, where
435 the thickest and most densely stained layer appears to be in what would be the anterior dorsal arcuate
436 body layer, where we see little to no signal.

437 *Dopamine:*

438 Within the arcuate body, TH-immunoreactivity occupies a single layer in the posterior aspect of the
439 dorsal lobe (Fig. 6 - α-TH, dorsal), supplied by thin and sparse neurites stretching from the anteriorly
440 located tracts (Fig. S3k). This single layer of punctate terminals with anteriorly branching projections is
441 consistent with both *H. lenta* and *P. regius* (*35*), but otherwise the *U. diversus* dopaminergic arcuate

442 body layering appears simpler and more comparable to the jumping spider, *P. regius*, due to lacking the
443 additional wispy immunoreactivity in anterior layers as in *H. lenta*.

444 For the wolf spider, *H. lenta*, TH labelling reveals densely stained first and second-order optic neuropils
445 (*35*). In contrast we see a stark lack of immunoreactivity in anterior regions which would be expected to
446 contain the comparable neuropils in *U. diversus*.

447 *Serotonin:*

448 Immunostaining against 5-HT in the social huntsman, *Delana cancerides* shows two gross levels of
449 immunoreactivity in the arcuate body; a wide diffuse layer of puncta, and a thinner layer bordered by
450 dense puncta on each side, with columnar-like expression in between (*36*). Taken together as two
451 adjacent layers, this pattern is remarkably similar to that seen for our model species. In U. diversus,
452 serotonergic-immunoreactivity shows a faint layer in the posterior ventral arcuate lobe, and an anterior
453 ventral actuate sublayer broadly flush with minutely fine fibers (Fig. 6 - α-5-HT, ventral, Fig. S4k). The
454 dorsal arcuate lobe displays a robust and wide immunoreactive pattern resembling flagstone-pavement,
455 hinting at a columnar structure (Fig. 6 - α-5-HT, dorsal). This layers innervation greatly resembles that
456 seen for TDC2 in the same lobe (Fig. 6 - α-TDC2, dorsal).

457 *Octopamine / Tyramine:*

458 Both anterior and posterior sublayers of the ventral arcuate body exhibit TDC2 immunoreactivity (Fig. 6 -
459 α-TDC2, Fig. S5l,m). The posterior layer of this sublayer is saturated with diffuse puncta with the anterior
460 side showing faint minute columnar arrangement. The anterior sublayer has denser, garland-like
461 varicosities. In the dorsal arcuate body lobe, TDC2 immunoreactivity appears only in the anterior
462 sublayer (aABd), where it fully fills the span of this layer with robust staining resembling a series of
463 keystone-shaped columnar-like elements. Octopaminergic expression has been reported in the arcuate
464 body (labelled 'central body' in source) (*24*) of C. salei, where a parasagittal section shows strong
465 immunoreactivity in the ventral portion of both arcuate body lobes. We must imagine the respective
466 horizontal view, but it would appear by the gaps in immunoreactivity that a dorsal horizontal slice in C.
467 salei should show three general layers of AB staining, which is essentially what we see from a dorsal
468 plane in U. diversus.

469 *AllatostatinA:*

470 The pattern of arcuate body innervation by AstA+ neurons is in general agreement with findings from C.
471 salei and M. muscosa (*8*, *28*) where signal is prominent in the ventral arcuate lobe (ABv), with little to no
472 staining in the dorsal arcuate (ABd). Concerning the sublayers of the ventral arcuate lobe, AstA-
473 immunoreactivity is seen on the anterior aspect of the posterior ventral arcuate (posABv), and fully
474 encompasses the anterior ventral arcuate (antABv) (Fig. 6 - α-AstA). In a given sample, a series of
475 discernible units of immunoreactivity are seen in the posABv layer, suggesting the columnar organization
476 which is present, but generally obscured by the density of staining (Fig. S6k – arrowheads).
477
478 *Proctolin:*

479 Proctolin immunoreactivity is evident in all lobes and layers of the arcuate body (Fig. 6 - α-Proctolin, Fig.
480 S7l,m). In the ventral arcuate body (ABv), at the posterior ABV a line of intense terminals, underlayed by
481 diffuse puncta. Towards the dorsal end of the ventral arcuate body (ABv), the proctolin-immunoreactivity
482 in the posterior-most layer transforms into heavy garland-like columnar varicosities extending at an

483 anteriodorsal angle. This is in complete correspondence to the varicosities seen for this layer in *C. salei*
484 (*28*). In the anterior ventral arcuate (antABv), the anterior and posterior sublayers take on an intricate
485 mesh-like form, also with smaller flagstone formations. Between these two layers are fine palisade
486 neurites. Both sublayers of the dorsal arcuate (ABd) are also filled, but with a sparse field of fine puncta.
487
488 *CCAP:*

489 CCAP expression is strong in the posterior ventral AB layer with a fine mesh, punctate appearance which
490 seemingly contours the columnar structures on the anterior and posterior boundaries of this layer. The
491 anterior and posterior sublayers of the ventral AB are highlighted, with a decrease in staining within the
492 area between the sublayers (Fig. 6 - α-CCAP, ventral, Fig. S8h). In the anterior ventral AB, the anti-CCAP
493 expression is slightly finer and more punctate than in the preceding description. The staining appears
494 singular unlike in the posterior ventral AB – this might be reflective of expression in the area between
495 sub-layers within anterior ventral AB. Within the dorsal AB (Fig. 6 - α-CCAP, dorsal), only the posterior
496 layer has appreciable expression, showing a single, finely innervated but moderately thick layer hugging
497 the posterior boundary of the dorsal AB. CCAP-immunoreactive layers in U. diversus are comparable to
498 C. salei (*28*), as for both species the thickest staining layer is the most posterior one (ventral arcuate
499 body lobe), followed anterio-dorsally by a lesser layer, and with a thinner strand of intensely
500 immunoreactive boutons running through the more anteriorly located dorsal arcuate body lobe.
501
502 *FMRFamide:*

503 From both *C. salei* (26) and the giant house spider, *Tegenaria atrica* (18), a basic structure of the
504 FMRFamidergic arcuate body layers emerges, where the entire dorsal arcuate body lobe is suffused with
505 immunoreactivity, there is a sharp strand of garland-like varicosities giving way to the typical columnar
506 arrangement in the posterior dorsal arcuate body layer (posABd), and more diffuse, punctate
507 immunoreactivity in the anterior dorsal arcuate body layer (antABd). This pattern is approximately what
508 we see in *U. diversus*, with additional details made clear by access to a continuous stacked image
509 volume (Fig. 6 - α-FMRFamide).

510
511 It appears that the saturated signal within the ventral arcuate lobe is actually the result of an
512 innervation pattern which is stronger in the wall of each tubular-like sublayer, and weaker in the
513 interior. This can be seen from several specific planes which slice longitudinally through both sublayers,
514 revealing four layers, each being the boundary of one of the sublayers (Fig. 6 - α-FMRFamide, ventral). In
515 the dorsal arcuate body, the immunoreactivity is primarily in the posterior sublayer, having the heavy
516 varicosities at the ventral aspect, and keystone column pattern more dorsally (Fig. 6 - α-FMRFamide).
517 Relative to other examined spiders, the punctate pattern in the anterior sublayer is weakly present. The
518 arcuate body layering pattern of FMRFamide immunoreactivity is similar to that of CCAP.

519

520 **Tonsillar neuropil**

521 Within the historically non-descript central supraesophageal ganglion, we observed a synaptically dense
522 neuropil structure in *U. diversus*. Beginning in the planes dorsal to the mushroom bodies, this paired
523 structure is positioned directly on either side of the midline, and is centrally located, being medial to the
524 perimeter of the supraesophageal ganglion from both the lateral as well as anterior and posterior limits.

525 The half in each hemiganglion has an approximately ovoid appearance, particularly at the anterio-dorsal
526 end, while bridged at the posterior aspect. Between the two halves, at the midline, is a furrow which is
527 negative for synapsin-immunoreactivity, giving this neuropil, in conjunction with the synapsin-negative
528 zone, a likeness to tonsils when viewed from the horizontal optical planes (Fig. 7a, c – α-synapsin).

529 In individual anti-synapsin stains, a fiber tract traveling laterally adjoins this neuropil in the more dorsal-
530 posterior portions. By tubulin-immunoreactivity, it appears to bifurcate the structure below the bridge
531 in the dorsal portion (Fig. 7b). As evidenced by at least octopaminergic/tyraminergic co-staining, this
532 tract may be supplying input from yet another hitherto undescribed neuropil, the protocerebral bridge,
533 to be discussed below.

534 A subset of antisera for specific neuronal populations are instrumental in confirming this neuropil, as
535 their immunoreactivity is circumscribed by its boundaries, with little neighboring signal to obscure the
536 distinction (Fig. 7c). Most representative among these is serotonergic-immunoreactivity, exhibiting fine
537 varicosities which neatly fill the area. TDC2+ signal, indicating innervation from octopaminergic and
538 tyraminergic neurons, are also prominent in this neuropil. The relatively heavier terminals appear
539 stronger on the periphery, and when viewed in alignment with the 5-HT channel, resemble a division of
540 compartments, most notably in the ovoid regions where serotonin is found in an internal, core pattern,
541 with octopaminergic/tyraminergic signal as a shell (see Octopamine/Tyramine subsection).

542 There may also be a division in the anterior-posterior dimension as AllatostatinA-immunoreactivity is
543 more pronounced in the posterior bridging region, and sparsely punctated in the anterior ovoid zones
544 (Fig. 7c – α-AstA), while proctolin-immunoreactivity is limited to the posterior region (Fig. 7c – α-
545 Proctolin). FMRFamide immunostaining is diffusely present, particularly in the anterior-dorsal portions
546 of the tonsillar neuropil, but this is amidst broadly saturated signal from this antibody throughout the
547 supraesophageal ganglion.

548

549 **Protocerebral bridge**

550 Originating anterio-laterally and progressing posterior-medially through the ascending dorsal planes of
551 the supraesophageal ganglion is a banded neuropil structure which we will designate as the
552 protocerebral bridge. Wider in the lateral aspect, the structure tapers towards the medial end with the
553 thinnest, midline-crossing component only being apparent in specific neuronal subpopulation stains.
554 This is the dorsal-most neuropil seen in the interior of the supraesophageal ganglion before reaching the
555 dense cap of somata (Fig. 8a,b).

556 As with the previous neuropil, only a subset of antisera show immunoreactivity within this neuropil. The
557 most filling is GABAergic-immunoreactivity (by anti-GAD stain) which defines a nearly complete swath of
558 the neuropil with dense signal (Fig. 8b - α-GAD). Comparing further neuronal-subtype preparations
559 reveals that the protocerebral bridge has a layered structure. TDC2-immunoreactivity is pronounced
560 throughout the length of the protocerebral bridge, displaying heavy chains of puncta on the posterior
561 edge of the bridge (Fig. 8b - α-TDC2). Proctolin-immunoreactivity forms a tight, thinner band, primarily
562 at the medial end of the neuropil, comprised of fine puncta and is centrally located among the layers
563 (Fig. 8b - α-Proctolin). The acetylcholinergic pattern is a distinct thin layer on the anterior and posterior

edge, most clearly visible on the lateral portion of protocerebral bridge (Fig. 8b - α-ChAT). A faint section of AstA-immunoreactivity was also seen (Fig. 8b - α-AstA).

Posterior and ventral to the protocerebral bridge is an arching string of varicosities which reaches its apex just before the appearance of the dorsal arcuate body layer. We refer to this as the dorsal protocerebral commissure (dPCC) (Fig. 8b – arrows) and the neuronal subtype populations which show protocerebral bridge expression tend to also innervate this commissure. The strongest of these are octopaminergic/tyraminergic neurons (anti-TDC2) and proctolinergic neurons (anti-Proctolin) (Fig. 8b - α-TDC2, α-Proctolin). This pathway separates from the posterior-lateral contour of the protocerebral bridge, where there is an approximately triangular expansion of immunoreactivity before travelling medially, and passing just posterior to the edge of the tonsillar neuropil. A similar pattern, though of relatively lesser staining intensity is also seen for allatostatinA (Fig. 8b - α-AstA). Cholinergic-innervation is also apparent in the posterior arch, but is more subtle and in a single layer in the anterior domain, being less comparable to that of TDC2, Proctolin and AllatostatinA.

Additional supraesophageal observations:

Acetylcholine:

The most strongly ChAT-immunoreactive neurons are found in a 6-7 neuron cluster in the anterior column, medial to the cheliceral ganglia and just ventral to where the esophagus closes with the esophageal bridge (Fig. S1d).

The nature of this antibody, along with the abundance of this population made it not possible to describe the contribution of these individual populations to the immunoreactivity patterns within the neuropil. ChAT-immunoreactivity forms dense puncta abundant throughout the supra- and subesophageal ganglia (Fig. S1b-f). Compared to other immunostains in our study, the relatively uniform immunoreactivity throughout the neuropil, apart from a couple exceptions, does not clearly highlight specific structures.

The aforementioned globuli cells are visible anterio-dorsally to the level of the MB heads (Fig. S1g). Dorsal still to these appear two bright clusters, each containing two ChAT+ neurons (Fig. S1h). The anterior medial cluster are more typically sized (Fig. S1h - small arrow), while the lateral pair are the largest ChAT+ neurons we observed in *U. diversus* (Fig. S1h - large arrow). A concentrated line of cholinergic somata (~16-20) are present on the thinner band of cell bodies posterior to the arcuate body (Fig. S1h - small arrowheads), and at the far dorsal end a roughly equal amount are dispersed medially (Fig. S1i).

Two strings of ChAT+ varicosities arc with their zenith at the posterior midline, before the arcuate body. The posterior arc has stronger immunoreactive puncta and travels ventrally to the dorsal arcuate body (ABd). The wider anterior arc is made of fine parallel fibers and appears to comprise a part of the protocerebral bridge-like neuropil (Fig. 8b, Fig. S1i – arrows).

GABA:

GAD-immunoreactive neurons are also found abundantly throughout the anterior side of the brain, within the deep furrow of somata (Fig. S2d,f). One feature which is visible with this antibody is the

609 protocerebral bridge neuropil, which is robustly innervated by GAD-immunoreactivity. This signal aligns
610 with the full breadth of synapsin-immunoreactivity corresponding to this neuropil (Fig. S2g). A bulbous
611 shape is outlined by GAD-immunoreactivity, and overlays with the apex of the mushroom body heads in
612 the standard brain volume (Fig. S2e - arrow), suggesting that the globuli cells contain GABAergic innerva-
613 tion. Anterior to the tonsillar neuropil there is a sharp band of GABAergic cell bodies arranged in the
614 medio-lateral direction (Fig. S2f). Further in the dorsal subpraesophageal ganglion, there is a distinctive
615 ascending column of GAD+ somata on each of the hemiganglia which stand out due to not being imme-
616 diately flanked by other GABAergic neurons to each side (Fig. S2g). Such a grouping also seems present
617 in *C. salei* (*37*) and *P. tepidariorum* (*43*).
618
619 *Dopamine*:
620
621 Continuing dorsally, the next clusters of TH+ neurons are at the level of and dorsal to the closure of the
622 esophagus. The dorsal cluster is a tandem pair of two neurons each (Fig. S3f – arrows), posterior to
623 which are seen a band of neurites and adjoining immunoreactivity on each side, representing the
624 stomodeal bridge (STb, as per (*44*), Fig. S3f – asterisk). These tandem neurons match well to the posi-
625 tioning of "Group 3" neurons in the wolf spider, *H. lenta* (*45*). Similarly, to the "Group 3" members, the-
626 se neurons appear to contribute substantially to the stronger immunoreactivity surrounding the esoph-
627 ageal bridge.
628
629 The opisthosomal neuromere is supplied by a grouping of neurons found in the somata ventral to it, and
630 the lateral borders of this structure are highlighted by intensely staining tracts of TH-immunoreactivity,
631 while the interior has a mesh of varicosities, including its own fine commissures (Fig. S3f - brace). Just
632 dorsal to the neurons in the vicinity of the bridge, are the second cluster comprised of 5 TH+ somata
633 (Fig. S3g – arrows). These appear to be a similar population to "Group 2" neurons in *H. lenta*, which are
634 more numerous, but share the description of projecting posteriorly and slightly dorsally to the edge of
635 the supraesophageal ganglion (*45*).
636
637 The final cluster of the ventral end of the supraesophageal ganglion appear laterally as 4 neurons per
638 hemiganglia (Fig. S3g, h – arrow). This is approximately at the level where the "ventral-most TH-ir tract"
639 (using terminology in (*45*)) joins in an arch above the esophagus (seen clearer medially in Fig. S3g), the
640 third and most posterior bridging of that channel. These neurons are likely the counterpart to those la-
641 belled "Group 1" in *H. lenta* (*45*). As for *H. lenta*, these neurons contribute heavily to the tracts running
642 briefly posteriorly, and then medially to course through the protocerebro-dorsal tract (PCDt), ventral to
643 the arcuate body. Interestingly, a subset (potentially 2 of the 4) of these lateral subpraesophageal neu-
644 rons also produce descending projections (Fig. S3f – arrowhead), which join the "intermediate TH-ir
645 tract" (as defined in (*45*)). In short, the TH+ somata of the ventral supraesophageal ganglion are remark-
646 ably similar in organization and projection patterns to those reported in the wolf spider, with the only
647 discrepancy being fewer neurons found for each cluster in *U. diversus*.
648
649 About the level of the arcuate body there are a doublet and singlet (Fig. S3i,j – arrowhead and arrow,
650 respectively) of TH+ neurons, totaling three per side, which are present on anterior facing somata field.
651 These neurons, and particularly the lone medial ones (Fig. S3i,j – arrow), form extensive projections
652 within this sector of the supraesophageal ganglion. The doublet population forms a wide arc laterally
653 and ventrally, which melds into the PCDt, wherein its individual fibers can no longer be discerned. The
654 single neurons project slightly dorsally, also contributing to the PCDt, the looped and crossed portion
655 visible at the posterior midline (Fig. S3i), and appear to also be the source of innervation to the arcuate
656 body layer appearing dorsally (Fig. S3k). In *H. lenta*, a 'triad' of neurons is described at this area, with a

subset projecting to the arcuate body layer and the others connecting with the PCDt (*45*). Apart from the closer clustering in this spider, the description and number, down to the division of targets matches our findings for the described neurons in *U. diversus.*

A final, dorsal-most cluster of 2 – 3 neurons appears medially (Fig. S3k), anterior to the arcuate body. Despite very close confirmation of the preceeding somata, these neurons were not reported in either *H. lenta* or *P. regius* (*45*), and therefore may be particular to *U. diversus*. The projections of these neurons are more difficult to follow due to the mass of neurites which they overlap through just ventrally, but it appears that at least the most prominent of their neurites actually continue to descend ventrally, crossing below the PCDt in the posterior direction before turning sharply to continue into the ventral supraesophageal and potentially even the subesophageal ganglion. At this same dorsal plane as these somata, densely fine varicosities are evident in an area positioned correctly to potentially overlap with the protocerebral bridge neuropil (Fig. S3k), but this has not been confirmed with a reliable alignment.

Serotonin:

5-HT-immunoreactivity is prominent in the posterior bridging area dorsal to the esophageal passage, as well as the laterally adjacent tissue (Fig. S4e), and not as apparent in anterior stomodeal bridge. Serotonergic fibers form a distinctive circular tract pattern around the midline of the supraesophageal ganglion (Fig. S4f), not as clearly seen with any other neuronal-subtype stain. Bright puncta are also visible at several points surrounding the intensely synapsin-immunoreactive protocerebral tract, suggesting that serotonergic projections are running among this fiber bundle (Fig. S4f). The semi-circular tracts bending medially (Fig. S4g), before a chiasm of seemingly all three directions is seen immediately dorsal (Fig. S4h). On the posterior end is a diffuse umbrella-like band of varicosities (Fig. S4h, i).

Continuing dorsally from this point, the innervation spreads to fill a kidney shaped structure which is pierced by a circular spot lacking synapsin-immunoreactivity (Fig. S4i – brace) – with such internal synapsin-negative areas assumed to be tracheal passageways or potentially glia. It is difficult to ascertain to what degree the innervation in this region is continuous with that of dorsally located features.

A pair of strongly immunoreactive 5-HT neurons (one for each hemiganglion) (Fig. S4j – arrows) are found medially, at the plane of the MB heads, and appear to send a neurite into a varicose-filled region pinned in by the MB bridge to the posterior and lateral sides, and the cell body furrow anteriorly (Fig. S4j). Ventrally this region leads to the aforementioned hagstone structure. Dorsally, the immunoreactivity can be followed until the very strikingly defined contours of the tonsillar neuropil, which has been described (Fig. 7).

For *C. salei* (*46*), additional clusters of serotonergic neurons were reported in the dorsal supraesophageal ganglion, but apart from a given cluster (Fig. S4k – arrows) we have not been able to reliably distinguish groupings within the dorsal somata.

Octopamine/Tyramine:

In the anterior wall of somata spanning from the frontal plane at the level of cheliceral neuropil to the fusion of the esophageal bridge are atleast 15-20 TDC2+ neurons, of varying size and staining intensity (Fig. S5f,g). This number corresponds closely to the counts for *C. salei* in the same region (*47*, *48*). TDC2-immunoreactivity is prominent in the stomodeal bridge and adjacent areas, and at this plane two lateral

704 bands of immunoreactivity appear which do not correspond to a clear demarcation in the synapsin
705 channel.
706
707 A variant of the subesophageal tract arrangement is reprised in the opisthosomal neuropil, where in-
708 tense boutons line a tract running parallel to the midline between hemiganglia to close a loop at the
709 posterior end (Fig. S5f, g – arrow), while also giving rise dorsal and laterally to a concentric ladder-like
710 structure with tracts laying in the anterior-posterior direction (Fig. S5h – brace).
711 A diagram from C. salei points to octopaminergic expression in the interior supraesophageal ganglion, as
712 a frontal slice indicates two areas of octopaminergic-immunoreactivity, both referred to as
713 "protocerebral neuropil" – suggesting the use of this term to be a general placeholder for non-descript
714 areas within the supraesophageal ganglion (*48*). We find TDC2-immunoreactivity strongly in the umbrel-
715 la-like posterior region also innervated by 5-HT (Fig. S5i), and sparser puncta within the bounds of the
716 hagstone neuropil. Dorsally, the signal remains strong within the interior, and prominent in an anterio-
717 medial stretch hemmed in by the mushroom bodies, as well as thin strands which run along the lateral
718 periphery (Fig. S5j). TDC2-immunoreactivity is also found in the tonsillar central neuropil, where it is
719 substantial throughout, but particularly strong in a peripheral type of shell pattern, especially when
720 aligned to 5-HT staining which respectively forms the core (Fig. S5k).
721
722 We have described above how TDC2-immunoreactivity heavily marks the protocerebral bridge, as well
723 as a commissure connecting posterio-dorsally (Fig. 8, Fig. S5l). Seyfarth and colleagues (*48*) report
724 octopamine-immunoreactivity revealing "fine varicose fibers in protocerebral bridge". As this references
725 a single cropped micrograph, it is difficult to orient and draw a comparison with confidence to the
726 neuropil which we are describing as the protocerebral bridge. A final detail of interest concerns a string
727 of puncta which extend from the protocerebral bridge to the tonsillar neuropil (Fig. S5l and inset) –
728 which could correspond to tract highlighted by tubulin-immunoreactivity (Fig. 7b) – revealing a putative
729 pathway between these neuropils.
730
731 Interestingly, earlier reports indicated no octopaminergically immunoreactive somata within the
732 protocerebrum in *C. salei* ((*47*) reprinting table from Dunker 1992, (*49*)). In *U. diversus,* a series of TDC2+
733 neuronal cell bodies are visible in the anterior half of the far dorsal cap of somata covering the
734 supraesophageal ganglion, with some TDC2+ somata also being present in the thinner layer of cells pos-
735 terior to the arcuate body (Fig. S5m – arrow). Given that TDC2 also should be present in tyraminergic
736 neurons which can be octopamine-negative, these findings may be consistent with the picture for *C.*
737 *salei*, or alternatively may reveal that *U. diversus* has octopaminergic populations which are lacking in
738 the wandering spider.
739
740 *AllatostatinA*:
741
742 In *U. diversus*, strong AstA-immunoreactivity is present on the posterior side of where the esophagus
743 closes, where a commissure is also seen crossing (Fig. S6f). Moving dorsally, this gives way to even more
744 synaptically dense areas, eventually highlighting the circular structure circumnavigated by thin projec-
745 tions, and forming an umbrella-like structure at the posterior side (Fig. S6g)– which is more comprehen-
746 sibly illuminated by anti-5-HT staining (Fig. S4g).
747
748 Heavy AstA-immunoreactivity was noted in the central/medial supraesophageal ganglion, for which
749 names of distinct regions and neuropils have been lacking (*50*). The best view of staining in this region is
750 a coronal slice, making a direct alignment to our images challenging, but the fact of substantial AstA-
751 immunoreactivity within the interior of the supraesophageal ganglion is consistent in *U. diversus* (Fig.

752 S6h). Within this plane the MB hafts are innervated, as previously detailed (Fig. 3), and ~7 AstA+ neurons
753 are present in the anterio-medial channel (Fig. S6h – arrows).
754
755 One structure that we identify are the tonsillar neuropils, the form of which AstA-immunoreactivity
756 abundantly fills out, resembling similar patterns as seen with 5-HT and TDC2 (Fig. S6i, Fig. 7c). A pair of
757 large, intensely stained AstA+ neurons are present alongside the neuropil, deep and medial within the
758 furrow of somata, and whose neurites enter the anterior aspect of the adjoining tonsillar neuropil (Fig.
759 S6i). The most dorsal AstA+ somata are a pair found laterally once the arcuate body emerges (Fig. S6j).
760
761 Contrary to the jumping spider (*51*), we did not see AstA-immunoreactive somata in the posterior cell
762 layer adjacent to the arcuate body. This region is prone to damage during preparation, but nevertheless,
763 AstA+ neurons were not seen here in any of our samples.
764
765 *Proctolin*:
766
767 On the posterior edge of the STb there is a thin Proc+ commissure while the anterior edge of the STb is
768 highlighted by a bolder vein of varicosities (Fig. S7e). Medial to the synapsin-negative channel through
769 which the protocerebral tract rises, there is a band of proctolin-immunoreactivity which occupies a
770 space that is not thoroughly labelled by any other target of this study (Fig. S7f).
771
772 A cluster of small, brightly immunoreactive proctolin+ neurons are evident at the level of the MB hafts
773 (Fig. S7g), with less immunoreactive but larger somata appearing dorsally around the MB heads (Fig. S7i
774 – arrow). Posterior to the cup-shaped synaptic-density formed by the MB hafts continuing with the rest
775 of the MB is a crescent of Proc-immunoreactivity (Fig. S7h), which also appears present in *C. salei* (*52*).
776 Here there is signal in the posterior, midline-spanning umbrella structure observed for 5-HT and TDC2,
777 as well as fine varicosities in the hagstone neuropil.
778
779 Just dorsally past the level of the MB heads, a strand of varicosities forms anteriolaterally (Fig. S7j –
780 brace) travelling into the center and splitting into a delta with one branch pointing medially, while the
781 other posteriorly (Fig. S7k). Dorsal still, this strand disappears and is overlayed at the delta by the arch-
782 ing varicosities which will form the dorsal posterior protocerebral commissure (Fig. S7l), as has been de-
783 scribed above.
784
785 At the plane of the protocerebral bridge Proc+ expression, 3-4 proctolin neurons are seen anteriorly,
786 near the midline (Fig. 8 – α-Proctolin, dorsal). Dorsal to this neuropil in the cap of somata, another 10 or
787 so clearly Proctolin-immunoreactive somata are dispersed centrally and laterally (Fig. S7m).
788
789 *CCAP*:
790 In general, CCAP-immunoreactivity resembles anti-ChAT staining in the sense that CCAP signal in the
791 supraesophageal ganglion is composed of intense but isolated puncta, showing expression in many are-
792 as, but generally lacking concentration in any given area (Fig. S8d,e). CCAP-immunoreactivity highlights
793 the ventral trajectory of the PCDt more prominently than other immunostains (Fig. S8f – arrow).
794
795 CCAP+ somata are numerous in the dorsal supraesophageal ganglion. They are found clustered posteri-
796 orly as well as directly dorsal to the ventral AB. A number of other CCAP+ somata which are spaced sin-
797 gularly apart from each other are present medially and anterior to the level of the dorsal arcuate body
798 (Fig. S8h). While CCAP expression has been identified in pre-optic neuropil (*50*), we could not discern
799 optic pathway expression reliably above background.

FMRFamide:

FMRFamide-immunoreactivity is saturated throughout the supraesophageal ganglion, making the boundaries of individual features difficult to ascertain (Fig 17F, G). A similarly immunoreactively-dense appearance was presented from slice work in *C. salei* (*52*). At the apex of the protocerebral commissure, ventral to the dorsal arcuate body (ABd), is an approximately rectangular FMRFamide-immunoreactive band (Fig. S9g – brace), representing a pattern of immunoreactivity which was not salient for any of our other immunostained targets.

FMRFamide+ neurons are numerous and fairly evenly dispersed at the dorsal cap of the supraesophageal ganglion (Fig. S9h). They are found in the area posterior and dorsal to the arcuate body layer, as well as somewhat larger somata present in the anterior portion of the tissue. Again, while the fainter FMRFamide+ neurons may not be fully apparent to us, the bright ones are comparable to the number and distribution reported for *C. salei* (*53*).

Discussion:

Almost the entirety of spider CNS literature has been studied from tissue slices, with few examples of whole-mounts (*8*, *9*, *23*, *35*). Our ability to observe novel structures and make comparisons between innervation patterns was aided by whole-mount preparation and averaged brain alignment. Furthermore, imaging and alignment of many neurosignaling molecule stains in a single species was clarifying for the identification of novel structures, as a subset of stains crystalized putative boundaries. While nine spider species have been the subject of examination for the expression pattern of an individual neurosignaling molecules (*8*, *14*, *15*, *17*, *35*, *36*) the wandering spider, *C. salei,* is essentially the only species prior to the current work to have had multiple targets annotated. Given the utility of specific stains for understanding of neuropil structures, tracts and other features, this atlas provides a rich source for comparative anatomy in an orb-weaving spider, *U. diversus*, while also extending knowledge of a number of different neurosignaling pathways for spiders at large.

Mushroom bodies

As evident from synapsin volumes, the mushroom bodies of *U. diversus* are the most salient feature in the central supraesophageal ganglion. The *U. diversus* MBs have a complete appearance, exhibiting an attached haft region similar to visually-dependent spiders (*9*), and to which we find evidence of innervation, albeit from an unknown origin. Historically, the MBs have at times been referred to as the third-order visual neuropil, and have been discussed in the context of the visual pathways, which form the subject of a substantial portion of the spider nervous system literature (*8*, *9*, *21*, *39*, *42*, *54*). The optic neuropils of *U. diversus* are diminutive, which is consistent with hunting through mechanosensation on a web. While we employed several neurotransmitter stains which have identified upstream optic pathway elements (e.g. medulla, lamellae) in other species, these first and second-order structures were not evident even in preparations where the labile tissue of the secondary pathway was intact. The diminished nature of the optic pathways, but simultaneous presence of a distinct mushroom body structure in *U.* diversus raises an incongruence concerning the role of the mushroom body. A growing literature is suggestive of a deeper complexity, as examples of both cursorial and web-based

spiders can be found which either have or lack MBs (*9*, *20*). The fact such synaptically dense structures persist in spider species whose visual capacities seem all but irrelevant to their lifestyle indicates the sensory input to the mushroom bodies may differ between species. The mushroom bodies of insects, as most granularly understood in *Drosophila melanogaster*, were originally considered to be olfactory integration centers, and while remaining the most apparent input, subsequent studies have shown this center to also process multiple sensory modalities and influence behaviors not directly related to olfaction (*55*). Evolutionary pressures on certain species may also force a 'modality switch', as evidenced by the whirlygig beetle, *Dineutus sublineatus*, which has lost antennal lobes and instead have mushroom bodies supplied by the optic lobe, displaying a transition from olfactory to visual processing (*56*). An alternative hypothesis would be that mushroom bodies in web-building species may integrate other sensory information, such as mechanosensation, relevant for web activities – which may also necessitate learning and memory processes. Closer identification and annotation of the innervation patterns of non-visual sensory streams leading to the MBs would strengthen such a viewpoint.

Arcuate body

The arcuate body, being unmistakable and consistently present among species, is perhaps the best detailed structure in the spider brain, particularly in regards to innervation by neurotransmitter subtype populations. By aligning volumes to a common reference, the present methodology allowed for disambiguation of the layers innervated by specific signaling molecules and understanding of where these patterns overlap. In *U. diversus*, we confirmed two broad lobular divisions, which each contain an additional two major layers, supporting a number of structural motifs. Generalizing for the arcuate body innervation patterns in *U. diversus* of specific neuronal populations, as compared to *C. salei* and a few other species, one can conclude that there is a great degree of similarity, in the relative arrangement of the gross layers, and even in certain fine structural details. In comparative studies, the arcuate body has been found to compose a roughly proportionate percentage of the brain across the species examined – be they web-builders or visually-based hunters (*19*, *57*). It is thus assuredly involved in various spider behaviors, and it will be illuminating to unravel how this conserved circuitry is harnessed for different ethological needs. The arcuate body lobes have been previously compared to the two nested neuropils known generally in insects as the upper and lower central bodies (*28*, *36*, *58*) and the architecture of *U. diversus* supports these observations, showing obvious layering intersected by perpendicular neurites and columnar-like patterns.

Novel neuropils

Structures which are conspicuous in our orb-building model spider but potentially not in hitherto studied cursorial species may be indicative of areas which are important for web-building. Nevertheless, it is not currently clear whether similar neuropils are absent in other species, or if they were simply not apparent by prior techniques. Apart from the mushroom bodies and arcuate body, neuropil structures within the interior of the supraesophageal ganglion have not been well distinguished. Multiple works refer to a “central” or “protocerebral neuropil” seemingly in regards to the undifferentiated mass of the supraesophageal ganglion as a whole. The image volume produced by aligning whole-mounted synganglia immunostained against synapsin instead reveals an intricacy of structures, beyond those described here. Two of the most conspicuous neuropils found in the dorsal supraesophageal ganglion are the protocerebral bridge and the tonsillar (central) neuropils.

Our description and multi-target staining of the protocerebral bridge provides the clearest demonstration of such a structure in the spider to date. The use of this name has a precedent within the spider literature (*24*), although whether the referent structure in *C. salei* is the same as in our model species will require additional clarification. Whether or not the authors chose this name in order to draw a parallel to the insect protocerebral bridge is likewise ambiguous. The protocerebral bridge is a core constituent of the insect central complex (*59*), but demonstrations in non-insect arthropods are scarcer. Examples have been found in crustaceans, such as the crayfish *Cherax destructor* (*60*), as well as rock slater *Ligia occidentalis* and sidestriped shrimp *Pandalopsis dispar*, the latter of which shows widely arching, layered structure, stopping short of the midline (*61*). We find such an anterior midline structure in *U. diversus*, possessing layers as revealed by antisera to neurotransmitter populations, and having a thinning (to absent) midline crossing, reminiscent of disjointed PCBs in certain insects including cockroaches and moths (insectbraindb.org). A columnar pattern is not as of now forthcoming in the *U. diversus* protocerebral bridge, which may be a consequence of density, as columnar structures can be difficult to see by immunohistochemistry (*59*), demonstrated by the fact that the PCB is no more evidently columnar in cockroach than in the sidestriped shrimp when visualizing with the same antisera to TRP (*61*).

A final undescribed neuropil which was apparent in the supraesophageal ganglia was the centrally located, tonsillar neuropil. Based on the ovoid form, paired appearance close to the midline, and close proximity to the unpaired midline neuropil(s) (arcuate body- ABv and Abd), the tonsillar neuropil bears a general resemblance to the noduli, a smaller constituent of the central complex of pterygote insects (*59*). To our knowledge, an analogous structure to this region has not been documented in non-insect arthropods. Unlike the arcuate body and protocerebral bridge, neither a columnar nor layered architecture is apparent in the tonsillar neuropil, although specific neurosignaling molecule stains concentrate in certain domains, including a potential core and shell, as well as an anterior/posterior division. Noduli in insects also contain compartments, and the presence of layering is species-dependent (*59*).

A spider central complex?

Based on gross morphology, it is tempting to speculate that these novel neuropils, when considered along with each individual lobe of the arcuate body may form an equivalent to a central complex in *U. diversus* (Fig. 9). The central complex of insects is innervated and interconnected by tangential, columnar and pontine neurons in insects, forming a consistently identifiable relationship between neuropils across species (*62*). Apart from the crayfish (*60*), where neurons supplying the protocerebral bridge also appear to innervate the central body, knowledge of intra-complex connectivity is lacking in non-insect arthropods. A detailed study of the Onychophoran (velvet worm, sister to arthropods) brain revealed several brain structures that appeared anatomically similar to those observed in arthropods (*63*). However, whether these ganglia are functionally homologous is a matter of debate. Mushroom body anatomy varies greatly across arthropods (*38*). While the Onychophoran central body is thought to be truly homologous to the insect central body (and arcuate body in chelicerates), the frontal body (which has gross similarities to the insect protocerebral bridge) appears to lack columnar organization and lacks an obvious connection to the central body. No noduli were observed in the Onychophoran brain, nor have they been observed in arthropod brains outside of insects. The tonsillar neuropils we observe appear to share connectivity with the protocerebral bridge, but no clear connectivity with the arcuate body. Since noduli have not been observed in non-insect arthropods (*59*), the anatomy of the

tonsillar neuropils may be coincidental, or convergently evolved to execute functions relevant to the protocerebral bridge.

Given that many of the antisera used in this study do not consistently trace neurites, the connectivity patterns between the neuropils of *U. diversus* supraesophageal ganglion require clarification. Future investigations employing techniques capable of isolating the ramification patterns of individual neurons within the context of the present neuropils in *U. diversus* will be essential to defining whether these currently disparate structures are truly members of a complex, and to what extent the connectivity is comparable to better studied arthropods. As a unit, the modules of the central complex integrate a variety of information including present orientation with respect to a salient environmental feature, memory of a heading goal, and speed – which can accomplish tasks such as path integration, migration, and other goal-directed movements relevant to particular species (*64*). While occurring in a much more spatially constrained context, these informational components could likewise be vital for organizing movements during the process of web-building, as well as maintaining a conception of the 360-degree web space as the spider strikes out to capture prey and subsequently return to the resting position at the hub. In such a scenario for *U. diversus* and other orb-weavers, updates to present heading would likely be provided by mechanosensation, rather than optic flow, which has been shown to contribute even in insects which otherwise predominantly employ vision (*65*). The columnar segments of the central bodies maintain a representation of the flies orientation within the environment in regards to a given feature (*66*). Although the exact number of columnar elements in the spider arcuate body lobes has not been established, they are numerous (with some suggestions in the thousands (*58*)), which could support a much more refined representation of the animal's radial self-made realm, underlying the often-stunning speed and precision with which the spider builds and navigates.

976 **Materials and Methods:**

977 **Animals**

978 Adult female *Uloborus diversus* spiders were used for all neuroanatomical preparations. Spiders were
979 housed freely in a green house, or as 1 – 4 individuals in acrylic habitats within the lab, under 12:12 light
980 dark cycles.

981 **Immunohistochemistry**

982 Spiders were anesthetized with carbon dioxide, and rapidly dissected in HEPES-buffered saline (HBS)
983 with 0.1% TritonX, and prepared for immunostaining following the methodology described by Ott
984 (2008). Samples were fixed overnight in ZnFA (2%) at 4° C. The following day samples were washed 3 x
985 10 minutes in HBS + 0.1% TritonX on a nutator. Samples were dehydrated in 80% methanol/20% DMSO
986 for 1 hour and 30 minutes, followed by 30 minutes in 100% methanol. A series of 5 minute incubations
987 in 90%, 70%, 50%, 30%, and 0% methanol in 0.1 M Tris was applied and the samples were blocked in 5%
988 normal goat serum, 1% DMSO, in PBS with 0.1% Triton (PBST) for at least 1 hour. Primary antibodies
989 were incubated for 3-5 days on a nutator at 4° C, before being washed with PBST for 3 x 15 minutes.
990 Secondary antibodies were applied in blocking solution and incubated for 2-3 days on a nutator at 4° C.
991 Secondary antibodies were washed off with 3 x 15 minutes washes with PBST, including DAPI (1:1000) in
992 one of the wash steps. The sample was dehydrated for mounting through a glycerol series of 2%, 4%,
993 8%, 15%, 30%, 50%, 70%, and 80% glycerol in 0.1 M Tris for 20 minutes each. Nutation was performed
994 for 2% through 15%, but only occasional hand agitation for the remaining steps. The sample was
995 protected from light. Following 30 minutes of washing with 100% ethanol, most of the ethanol was
996 pipetted off and the sample was underlayed with methyl salicylate, and allowed to sink, where it was
997 stored in the dark at room temperature until mounting.

998 For anti-TH staining, samples were dissected in Millonig's buffer with 0.1% TritonX, and fixed in 4% PFA
999 in PBS for 45 minutes at room temperature while nutating. Immunostaining proceeded as described by
1000 Auletta et al., (2019). Samples were dehydrated and mounted in methyl salicylate by the steps used
1001 above for all other antibodies.

1002

Reagent	Host Species	ID	Dilution
Primary Antibodies			
3C11 (anti SYNORF1)	Mouse	3C11 (DHSB) RRID: AB_528479	1:100
Anti-Synapsin I antibody - Synaptic Marker (ab64581) *polyclonal antibody – new stocks are not effective*	Rabbit	ab64581 (Abcam)	1:500
Anti-β-Tubulin3	Chicken	TUJ (Aves Labs)	1:250
Anti-GAD	Rabbit	G5163 (Sigma-Aldrich)	1:1000
Anti-TH	Mouse	22941 (ImmunoStar)	1:100
Anti-ChAT	Mouse	ChAT4B1 (DHSB)	1:10
Anti-5-HT	Rabbit	20080	1:25

		(ImmunoStar)	
Anti-TDC2	Rabbit	pab0822-P (CovaLab)	1:250
Anti-Proctolin	Rabbit	orb122514	1:250
Anti-AllatostatinA	Mouse	5F10-s (DHSB)	1:10
Anti-Cardioactive peptide	Rabbit	ab58736 (Abcam)	1:250
Anti-FMRFamide	Rabbit	ab15348 (Abcam)	1:250
Secondary Antibodies			
488 Goat Anti-Mouse	Goat	A-11001 (ThermoFisher)	1:500
555 Goat Anti-Rabbit	Goat	A21428 (Invitrogen)	1:1000
Alexa Fluor 647 Goat Anti-Chicken	Goat	130-605-155 (Jackson)	1:1000
Alexa Fluor 647 Goat Anti-Horseradish Peroxidase (HRP)	Goat	123-605-021 (Jackson)	1:25

Imaging

U. diversus synganglia were balanced upright, by placing samples subesophageal ganglia-side down in a well of methyl salicylate. Wells were constructed by adhering nested metal washers to a glass coverslip or slide using cyanoacrylate glue. A coverslip was also adhered to the top of the outer washer. Samples were imaged using a Zeiss LSM700 or LSM880 confocal microscope, with a LD LCI Plan-Apochromat 25x/0.8 Imm Corr DIC M27objective (set to oil immersion), or a W Plan-Apochromat 20x/1.0 DIC D=0.17 M27 75mm water immersion objective, respectively.

Volume alignment

Alignment of confocal image volumes was performed using Elastix 5.0.1 (Klein et al., 2010, Shamonin et al., 2014). Registration was performed first by a rigid method using an affine transform with an adaptive stochastic gradient descent optimizer for 20000 iterations, with 40000 spatial samples at 5 resolution levels. This was followed by a non-rigid registration using a bspline transform with a standard gradient descent optimizer for 200000 iterations at 5 resolution levels and using the AdvancedMattesMutualInformation metric. This was followed by a non-rigid registration using B-spline transform with a standard gradient descent optimizer for 200000 iterations with 40000 spatial samples at 5 resolution levels and using the AdvancedMattesMutualInformation metric. Transformation matrices were established using the anti-synapsin stain as a registration channel. A preliminary subset of synapsin volumes were mutually transformed onto each other, and the brain sample for which the most satisfactorily aligned pairings resulted was selected as the reference brain, onto which all other subsequent image volumes were aligned. The standard brain depicted in the figures above is an averaged composite of 6 aligned synapsin volumes. The final transformation matrix generated by registration of the synapsin channel, was then applied to other channels present for each sample image volume (the neurosignaling target immunostains).

In limited cases, no satisfactory image volume alignment could be obtained based on the Elastix parameters specified previously. In these cases, we manually applied a small correction to the Elastix

output (the "moving image") using radial basis function (RBF) interpolation. First, several location correspondences were manually annotated in the reference and moving image. An additional N^3 regularly spaced location correspondences were automatically created where no manual annotation was present within a 100-pixel distance, with N=ceil[Image Axis Length / 100]. The moving image coordinates were subsequently transformed using RBF interpolation with a thin plate spline kernel.

Visualization

Annotations of neuropils were drawn using ImageJ and Napari (napari.org), and 3D renderings created using Imaris 10.1 (Oxford Instruments). Renderings of z-planes on to the 3D synapsin volume were created using VisPy (vispy.org)

1060 **References:**

1061

1062 1. B. el Jundi, S. Heinze, "Three-Dimensional Atlases of Insect Brains" in *Neurohistology and Imaging*
1063 *Techniques*, R. Pelc, W. Walz, J. R. Doucette, Eds. (Springer US, New York, NY, 2020;
1064 https://doi.org/10.1007/978-1-0716-0428-1_3), pp. 73–124.

1065 2. M. Zhang, X. Pan, W. Jung, A. R. Halpern, S. W. Eichhorn, Z. Lei, L. Cohen, K. A. Smith, B. Tasic, Z.
1066 Yao, H. Zeng, X. Zhuang, Molecularly defined and spatially resolved cell atlas of the whole mouse
1067 brain. *Nature* **624**, 343–354 (2023).

1068 3. M. Winding, B. D. Pedigo, C. L. Barnes, H. G. Patsolic, Y. Park, T. Kazimiers, A. Fushiki, I. V. Andrade,
1069 A. Khandelwal, J. Valdes-Aleman, F. Li, N. Randel, E. Barsotti, A. Correia, R. D. Fetter, V.
1070 Hartenstein, C. E. Priebe, J. T. Vogelstein, A. Cardona, M. Zlatic, The connectome of an insect brain.
1071 *Science* **379**, eadd9330 (2023).

1072 4. J. G. White, E. Southgate, J. N. Thomson, S. Brenner, The structure of the nervous system of the
1073 nematode Caenorhabditis elegans. *Philos Trans R Soc Lond B Biol Sci* **314**, 1–340 (1986).

1074 5. A. Adden, S. Wibrand, K. Pfeiffer, E. Warrant, S. Heinze, The brain of a nocturnal migratory insect,
1075 the Australian Bogong moth. *Journal of Comparative Neurology* **528**, 1942–1963 (2020).

1076 6. V. Althaus, S. Jahn, A. Massah, M. Stengl, U. Homberg, 3D-atlas of the brain of the cockroach
1077 Rhyparobia maderae. *Journal of Comparative Neurology* **530**, 3126–3156 (2022).

1078 7. D. Dreyer, H. Vitt, S. Dippel, B. Goetz, B. El Jundi, M. Kollmann, W. Huetteroth, J. Schachtner, 3D
1079 standard brain of the red flour beetle *Tribolium castaneum*: a tool to study metamorphic
1080 development and adult plasticity. *Front. Syst. Neurosci.* **4** (2010).

1081 8. P. O. M. Steinhoff, A. Sombke, J. Liedtke, J. M. Schneider, S. Harzsch, G. Uhl, The synganglion of the
1082 jumping spider *Marpissa muscosa* (Arachnida: Salticidae): Insights from histology,
1083 immunohistochemistry and microCT analysis. *Arthropod Structure & Development* **46**, 156–170
1084 (2017).

1085 9. P. O. M. Steinhoff, S. Harzsch, G. Uhl, Comparative neuroanatomy of the central nervous system in
1086 web-building and cursorial hunting spiders. *Journal of Comparative Neurology* **532**, e25554 (2024).

1087 10. W. G. Eberhard, The web of Uloborus diversus (Araneae: Uloboridae). *Journal of Zoology* **166**, 417–
1088 465 (1972).

1089 11. A. Corver, N. Wilkerson, J. Miller, A. Gordus, Distinct movement patterns generate stages of spider
1090 web building. *Current Biology* **31**, 4983-4997.e5 (2021).

1091 12. J. Miller, A. V. Zimin, A. Gordus, Chromosome-level genome and the identification of sex
1092 chromosomes in Uloborus diversus. *GigaScience* **12**, giad002 (2023).

1093 13. K. S. Babu, F. G. Barth, Neuroanatomy of the central nervous system of the wandering spider,
1094 Cupiennius salei (Arachnida, Araneida). *Zoomorphology* **104**, 344–359 (1984).

14. A. Schmid, C. Becherer, Distribution of histamine in the CNS of different spiders. *Microsc. Res. Tech.* **44**, 81–93 (1999).

15. M. Moon, E. K. Tillinghast, Immunoreactivity of Glutamic Acid Decarboxylase (GAD) Isoforms in the Central Nervous System of the Barn Spider, *A raneus cavaticus* . *Entomological Research* **43**, 47–54 (2013).

16. Y. Park, H. Kim, H. Kim, M. Moon, Fine structure of the CNS ganglia in the geometric spider *N ephila clavata* (A raneae: N ephilidae). *Entomological Research* **43**, 330–343 (2013).

17. H. Hwang, H. Kim, M. Moon, Immunocytochemical localization of GAD isoforms in the CNS ganglia of the cobweb spider, *A chaearanea tepidariorum* . *Entomological Research* **45**, 167–175 (2015).

18. R. Wegerhoff, O. Breidbach, "Comparative aspects of the chelicerate nervous systems" in *The Nervous Systems of Invertebrates: An Evolutionary and Comparative Approach*, O. Breidbach, W. Kutsch, Eds. (Birkhäuser Basel, Basel, 1995; http://link.springer.com/10.1007/978-3-0348-9219-3_9)vol. 72 of *Experientia Supplementum*, pp. 159–179.

19. P. Weltzien, F. G. Barth, Volumetric measurements do not demonstrate that the spider brain "central body" has a special role in web building. *Journal of Morphology* **208**, 91–98 (1991).

20. S. M. Long, "Spider Brain Morphology & Behavior," thesis, University of Massachusetts Amherst (2016).

21. F. A. Rivera-Quiroz, J. A. Miller, Micro-CT visualization of the CNS: Performance of different contrast-enhancing techniques for documenting the spider brain. *J Comp Neurol* **530**, 2474–2485 (2022).

22. E. Seyfarth, K. Hammer, U. Grünert, Serotonin-like immunoreactivity in the CNS of spiders. *Brain-Perception-Cognition. Stuttgart: Thieme*, 459 (1990).

23. A. Schmid, M. Duncker, Histamine immunoreactivity in the central nervous system of the spider Cupiennius salei. *Cell Tissue Res* **273**, 533–545 (1993).

24. E.-A. Seyfarth, K. Hammer, U. Spörhase-Eichmann, M. Hörner, H. G. B. Vullings, Octopamine immunoreactive neurons in the fused central nervous system of spiders. *Brain Research* **611**, 197–206 (1993).

25. A. Schmid, C. Becherer, Leucokinin-like immunoreactive neurones in the central nervous system of the spider Cupiennius salei. *Cell and Tissue Research* **284**, 143–152 (1996).

26. C. Becherer, A. Schmid, Distribution of g-aminobutyric acid-, proctolin-, Periplaneta hypertrehalosaemic hormone- and FMRFamide-like immunoreactivity in the visual ganglia of the spider Cupiennius salei Keys. (1999).

27. R. Fabian-Fine, U. Höger, E.-A. Seyfarth, I. A. Meinertzhagen, Peripheral Synapses at Identified Mechanosensory Neurons in Spiders: Three-Dimensional Reconstruction and GABA Immunocytochemistry. *J. Neurosci.* **19**, 298–310 (1999).

1130 28. R. Loesel, E.-A. Seyfarth, P. Bräunig, H.-J. Agricola, Neuroarchitecture of the arcuate body in the
1131 brain of the spider *Cupiennius salei* (Araneae, Chelicerata) revealed by allatostatin-, proctolin-, and
1132 CCAP-immunocytochemistry and its evolutionary implications. *Arthropod Structure & Development*
1133 **40**, 210–220 (2011).

1134 29. R. Fabian-Fine, S. Meisner, P. H. Torkkeli, I. A. Meinertzhagen, Co-localization of Gamma-
1135 Aminobutyric Acid and Glutamate in Neurons of the Spider Central Nervous System. *Cell Tissue Res*
1136 **362**, 461–479 (2015).

1137 30. R. Fabian-Fine, C. M. Anderson, M. A. Roush, J. A. G. Johnson, H. Liu, A. S. French, P. H. Torkkeli,
1138 The Distribution of Cholinergic Neurons, and their Co-localization with FMRFamide in Central and
1139 Peripheral Neurons of the Spider Cupiennius salei. *Cell Tissue Res* **370**, 71–88 (2017).

1140 31. E. A. Tarr, B. M. Fidler, K. E. Gee, C. M. Anderson, A. K. Jager, N. M. Gallagher, K. P. Carroll, R.
1141 Fabian-Fine, Distribution of FMRFamide-related peptides and co-localization with glutamate in
1142 Cupiennius salei, an invertebrate model system. *Cell Tissue Res* **376**, 83–96 (2019).

1143 32. E. E. Senior, H. E. Poulin, M. G. Dobecki, B. M. Anair, R. Fabian-Fine, Co-expression of the
1144 neuropeptide proctolin and glutamate in the central nervous system, along mechanosensory
1145 neurons and leg muscle in Cupiennius salei. *Cell Tissue Res* **382**, 281–292 (2020).

1146 33. B. Hanström, *Vergleichende Anatomie Des Nervensystems Der Wirbellosen Tiere: Unter*
1147 *Berücksichtigung Seiner Funktion, von Dr. Bertil Hanström... Mit 650 Abbildungen* (J. Springer,
1148 1928).

1149 34. S. Anton, H. Tichy, Hygro- and thermoreceptors in tip-pore sensilla of the tarsal organ of the spider
1150 Cupiennius salei: innervation and central projection. *Cell Tissue Res.* **278**, 399–407 (1994).

1151 35. A. Auletta, M. C. P. Rue, C. M. Harley, K. A. Mesce, Tyrosine hydroxylase immunolabeling reveals
1152 the distribution of catecholaminergic neurons in the central nervous systems of the spiders *Hogna*
1153 *lenta* (Araneae: Lycosidae) and *Phidippus regius* (Araneae: Salticidae). *J of Comparative Neurology*
1154 **528**, 211–230 (2020).

1155 36. N. J. Strausfeld, C. M. Strausfeld, R. Loesel, D. Rowell, S. Stowe, Arthropod phylogeny:
1156 onychophoran brain organization suggests an archaic relationship with a chelicerate stem lineage.
1157 *Proc Biol Sci* **273**, 1857–1866 (2006).

1158 37. F. G. Barth, *A Spider's World* (Springer, Berlin, Heidelberg, 2002;
1159 http://link.springer.com/10.1007/978-3-662-04899-3).

1160 38. G. H. Wolff, N. J. Strausfeld, Genealogical Correspondence of Mushroom Bodies across
1161 Invertebrate Phyla. *Current Biology* **25**, 38–44 (2015).

1162 39. N. J. Strausfeld, F. G. Barth, Two visual systems in one brain: Neuropils serving the secondary eyes
1163 of the spider Cupiennius salei. *Journal of Comparative Neurology* **328**, 43–62 (1993).

1164 40. C. Doeffinger, V. Hartenstein, A. Stollewerk, Compartmentalization of the precheliceral
1165 neuroectoderm in the spider Cupiennius salei: Development of the arcuate body, optic ganglia,
1166 and mushroom body. *Journal of Comparative Neurology* **518**, 2612–2632 (2010).

41. W. G. Eberhard, The ecology of the web ofUloborus diversus (Araneae: Uloboridae). *Oecologia* **6**, 328–342 (1971).

42. D. E. Hill, "The structure of the central nervous system of jumping spiders of the genus Phidippus (Araneae: Salticidae)," (1975).

43. H. Hwang, H. Kim, M.-J. Moon, Immunocytochemical localization of GAD isoforms in the CNS ganglia of the cobweb spider, chaearanea tepidariorum. *Entomological Research* **45**, 167–175 (2015).

44. P. O. M. Steinhoff, S. Harzsch, G. Uhl, Comparative neuroanatomy of the central nervous system in web-building and cursorial hunting spiders. *Journal of Comparative Neurology* **532**, e25554 (2024).

45. A. Auletta, M. C. P. Rue, C. M. Harley, K. A. Mesce, Tyrosine hydroxylase immunolabeling reveals the distribution of catecholaminergic neurons in the central nervous systems of the spiders Hogna lenta (Araneae: Lycosidae) and Phidippus regius (Araneae: Salticidae). *J Comp Neurol* **528**, 211–230 (2020).

46. E. Seyfarth, K. Hammer, U. Grünert, Serotonin-like immunoreactivity in the CNS of spiders. *Brain-Perception-Cognition. Stuttgart: Thieme* **459** (1990).

47. F. G. Barth, *A Spider's World* (Springer Berlin / Heidelberg, Berlin, Heidelberg; https://doi.org/10.1007/978-3-662-04899-3).

48. E.-A. Seyfarth, K. Hammer, U. Spörhase-Eichmann, M. Hörner, H. G. B. Vullings, Octopamine immunoreactive neurons in the fused central nervous system of spiders. *Brain Research* **611**, 197–206 (1993).

49. P. M. Dunker, Vorkommen und Verteilung biogener Amine im Zentralnervensystem der Jagdsoine Cupiennius salei Keyserling (Ctenidae, Araneae, Arachnida). *Diplomarbeit, Formal- und Naturwissenschaftliche Fakultät der Universität Wien*, 88 (1992).

50. R. Loesel, E.-A. Seyfarth, P. Bräunig, H.-J. Agricola, Neuroarchitecture of the arcuate body in the brain of the spider Cupiennius salei (Araneae, Chelicerata) revealed by allatostatin-, proctolin-, and CCAP-immunocytochemistry and its evolutionary implications. *Arthropod Structure & Development* **40**, 210–220 (2011).

51. P. O. M. Steinhoff, A. Sombke, J. Liedtke, J. M. Schneider, S. Harzsch, G. Uhl, The synganglion of the jumping spider Marpissa muscosa (Arachnida: Salticidae): Insights from histology, immunohistochemistry and microCT analysis. *Arthropod Structure & Development* **46**, 156–170 (2017).

52. C. Becherer, A. Schmid, Distribution of γ-aminobutyric acid-, proctolin-, Periplaneta hypertrehalosaemic hormone- and FMRFamide-like immunoreactivity in the visual ganglia of the spider Cupiennius salei Keys. *Comparative Biochemistry and Physiology Part A: Molecular & Integrative Physiology* **122**, 267–275 (1999).

1202 53. R. Fabian-Fine, C. M. Anderson, M. A. Roush, J. A. G. Johnson, H. Liu, A. S. French, P. H. Torkkeli,
1203 The distribution of cholinergic neurons and their co-localization with FMRFamide, in central and
1204 peripheral neurons of the spider Cupiennius salei. *Cell and Tissue Research* **370**, 71–88 (2017).

1205 54. N. J. Strausfeld, P. Weltzien, F. G. Barth, Two visual systems in one brain: Neuropils serving the
1206 principal eyes of the spider Cupiennius salei. *Journal of Comparative Neurology* **328**, 63–75 (1993).

1207 55. Y. Aso, D. Hattori, Y. Yu, R. M. Johnston, N. A. Iyer, T.-T. Ngo, H. Dionne, L. Abbott, R. Axel, H.
1208 Tanimoto, G. M. Rubin, The neuronal architecture of the mushroom body provides a logic for
1209 associative learning. *eLife* **3**, e04577 (2014).

1210 56. C. Lin, N. J. Strausfeld, Visual inputs to the mushroom body calyces of the whirligig beetle Dineutus
1211 sublineatus: Modality switching in an insect. *Journal of Comparative Neurology* **520**, Spc1–Spc1
1212 (2012).

1213 57. T. Napiórkowska, J. Kobak, The allometry of the arcuate body in the postembryonic development
1214 of the giant house spider Eratigena atrica. *Invert Neurosci* **18**, 3 (2018).

1215 58. U. Homberg, Evolution of the central complex in the arthropod brain with respect to the visual
1216 system. *Arthropod Struct Dev* **37**, 347–362 (2008).

1217 59. S. Heinze, Variations on an ancient theme — the central complex across insects. *Current Opinion in*
1218 *Behavioral Sciences* **57**, 101390 (2024).

1219 60. M. Utting, H.-J. Agricola, R. Sandeman, D. Sandeman, Central complex in the brain of crayfish and
1220 its possible homology with that of insects. *Journal of Comparative Neurology* **416**, 245–261 (2000).

1221 61. R. Loesel, D. R. Nässel, N. J. Strausfeld, Common design in a unique midline neuropil in the brains
1222 of arthropods. *Arthropod Structure & Development* **31**, 77–91 (2002).

1223 62. K. Pfeiffer, The neuronal building blocks of the navigational toolkit in the central complex of
1224 insects. *Current Opinion in Insect Science* **55**, 100972 (2023).

1225 63. C. Martin, H. Jahn, M. Klein, J. U. Hammel, P. A. Stevenson, U. Homberg, G. Mayer, The velvet
1226 worm brain unveils homologies and evolutionary novelties across panarthropods. *BMC biology* **20**,
1227 26 (2022).

1228 64. A. Honkanen, A. Adden, J. da Silva Freitas, S. Heinze, The insect central complex and the neural
1229 basis of navigational strategies. *J Exp Biol* **222**, jeb188854 (2019).

1230 65. D. Turner-Evans, S. Wegener, H. Rouault, R. Franconville, T. Wolff, J. D. Seelig, S. Druckmann, V.
1231 Jayaraman, Angular velocity integration in a fly heading circuit. *eLife* **6**, e23496 (2017).

1232 66. J. D. Seelig, V. Jayaraman, Neural dynamics for landmark orientation and angular path integration.
1233 *Nature* **521**, 186–191 (2015).

1234

1235

Acknowledgements:

G.A., A.C., and A.G. designed the research. G.A. performed all biological preparations. A.C. and G.A. wrote and optimized software parameters for volume alignment. G.A. and A.G. analyzed the data and wrote the manuscript. G.A. acknowledges funding from the NSF Postdoctoral Research Fellowships in Biology Program under Grant No. (2109747). A.C. acknowledges funding from the Johns Hopkins Kavli Neuroscience Discovery Institute Doctoral Fellows Program. A.G. acknowledges funding from NIH (R35GM124883). The authors declare that they have no competing interests. All data needed to evaluate the conclusions in the paper are present in the paper and/or the Supplementary Materials. Raw data files can be provided by A.G. Requests for files should be submitted to: agordus@jhu.edu.

Figure 1: Synganglion of *Uloborus diversus*.

(**A.**) 3D rendering of *U. diversus* (female) synganglion from averaged α-synapsin volume, oblique posterior-lateral (left) and oblique anterio-lateral (right) views (**B**.) 3D rendering of α-synapsin (green) and DAPI stained (blue) synganglion, posterior, lateral and anterior views (**C.**) Sequence of horizontal optical slices from averaged α-synapsin (gray) volume with averaged DAPI stains (blue), from ventral subesophageal ganglion (left) to dorsal end of supraesophageal ganglion (right). Compass abbreviations: A = anterior, P = posterior, D = dorsal, V = ventral, L = lateral, M = medial.

Figure 2: Overview of averaged α -synapsin immunoreactivity in whole-mount synganglion.

Sequence of optical horizontal sections from averaged α-synapsin volume, with top-right insets showing position of respective slice in a 3D full volume rendering (**A. – I**.) Subesophageal ganglion, beginning ventrally (**A.**) and progressing dorsally until (**I.**). Notable features include the leg neuromeres (LN1-4, for respective legs 1-4), pedipalpal neuropil (PdN), cheliceral neuropil (ChN), opisthosomal neuropil (OpN, which is still visible until (L.)), and the esophageal passage. (J. – T.) Supraesophageal ganglion, with marked features including the stomodeal bridge (STb), protocerebral tract, protocerebral commissure (PCC), hagstone neuropil (HsN), mushroom body (haft, body, and head), tonsillar neuropil, arcuate body (ventral and dorsal lobes, ABv and ABd, respectively), and protocereral bridge (PCB).

Figure 3: Mushroom bodies.

(**A.**) 3D rendering of mushroom body neuropil as annotated from averaged α-synapsin volume, dorsal (top) and oblique posterior (bottom) (**B.**) Maximum intensity projection of averaged α-synapsin volume, showing the mushroom bodies to be the most strongly immunoreactive structure in the supraesophageal ganglion (**C.**) Optical sections of the supraesophageal ganglion from an averaged α-synapsin volume (ventral (top) to dorsal (bottom). The haft, body and head regions of the MB are labelled (**D.**) α-βTubulin3 (magenta) immunoreactivity aligned with α-Synapsin volume (gray) (compare to bottom portion of previous subfigure) showing the arching form of the mid-line spanning mushroom body bridge (**E.**) AllatostatinA immunoreactivity (α-AstA, green) present in the MB haft (pink dotted line marking location of α-synapsin immunoreactivity) with arrows pointing to innervation from the posterior side (**F.**) α-βTubulin3 (magenta) and α-Synapsin (green) immunoreactivity in the supraesophageal ganglion at the plane where the mushroom body hafts appear (round, intensely immunoreactive). Arrows mark a fiber tract flanking the haft which could be the origin of the innervation in the preceding subfigure (**G.**) Tripart tract entering at the mushroom body head to fuse with the tract descending through the MB.

Figure 4: Visual pathways.

(**A.**) Immunostaining for α-HRP (magenta) for neuropil and use of DAPI (blue) for nuclei, arrows show the primary (▯) and secondary (▯▯) visual pathway extensions from the bulk of the supraesophageal tissue (**B.**) 3D renderings of synpasin-immunoreactivity in the dorsal supraesophageal ganglion, with tissue of the primary (▯) and secondary (▯▯) visual pathway visible.

1306

1307 **Figure 5: Arcuate body.**

1308 (**A.**) 3D rendering of arcuate body neuropil as annotated from averaged α-synapsin volume, posterior
1309 oblique, posterior, and anterior oblique views, left to right, respectively (**B.**) Individual 3D rendering of
1310 the ventral arcuate body lobe (ABv, dark green) and dorsal arcuate body lobe (ABd, light green), with
1311 magenta envelope representing space which would be occupied by the missing lobe in each image. Top
1312 row images are dorsal views, bottom row are oblique posterior (**C.**) Optical horizontal slices of α-
1313 synapsin immunoreactivity from the dorsal supraesophageal ganglion. Top image is relatively ventral to
1314 the bottom, and shows the ventral arcuate body lobe (ABv), while the bottom image features both the
1315 ventral and dorsal arcuate body lobe (ABd). Each lobe contains an anterior (ant.) and posterior (pos.)
1316 section, marked with yellow dashed lines (**D.**) Ventral (top) and dorsal (bottom) views showing aligned
1317 image volumes of Proctolin (α-Proctolin, yellow), Crustacean Cardioactive Peptide (α-CCAP, cyan) and
1318 FMRFamide (α-FMRFamide, red) immunoreactivity, demonstrating distinct structures as well as
1319 overlapping innervation of the arcuate body layers (**E.**) α-βTubulin3 (magenta) and α-Synapsin (green)
1320 immunoreactivity in the arcuate body (ventral to dorsal as top to bottom, respectively), with arrows
1321 marking where pronounced fiber tracts pass through the arcuate body layers (**F.**) Dorsal view of arcuate
1322 body showing layering in ABv and ABd (brace), for Proctolin (α-Proctolin, yellow) and
1323 Octopaminergic/Tyraminergic (α-TDC2, magenta) immunoreactivity which have overlapping but distinct
1324 innervation patterns in the anterior ABd.

1325

1326 **Figure 6: Arcuate body layers revealed by staining for specific neurosignaling populations.**

1327 Ventral (left column) and dorsal (right column) horizontal optical section views of the arcuate body
1328 (perimeter of whole arcuate body marked by dashed line) for GABAergic (α-GAD), Cholinergic (α-ChAT),
1329 Dopaminergic (α -TH), Serotonergic (α -5-HT), Octopaminergic/Tyraminergic (α-TDC2), AllatostatinA (α-
1330 AstA), Proctolin (α-Proctolin), Crustacean Cardioactive Peptide (α-CCAP), and FMRFamide (α-
1331 FMRFamide) immunoreactivity.

1332

1333 **Figure 7: Centrally-located, tonsillar neuropil.**

1334 (**A.**) 3D rendering of tonsillar neuropil as annotated from averaged synapsin immunovolume with
1335 posterior oblique, anterior oblique, and dorsal views, left to right (**B.**) Oblique horizontal optical section
1336 of supraesophageal ganglion with α-Synapsin (green) and α-βTubulin3 (magenta) immunoreactivity. The
1337 tonsillar neuropil is seen centrally, with the arrow denoting a fiber tract which passes medially across it
1338 (**C.**) Ventral and dorsal views of the tonsillar neuropil, as demarcated by dotted lines. Synapsin (gray),
1339 Serotonergic (α-5-HT, green), Octopaminergic/Tyraminergic (α-TDC2, magenta), Proctolin (α-Proctolin,
1340 yellow), AllatostatinA (α-AstA, green) and FMRFamide (α-FMRFamide, red) immunoreactivity.

1341

1342 **Figure 8: Protocerebral bridge neuropil.**

(**A.**) 3D rendering of protocerebral bridge neuropil as annotated from averaged synapsin immunovolume. (**B.**) Ventral and dorsal views of the PCB, as demarcated by dotted lines. Synapsin (gray), GABAergic (α-GAD, red), Octopaminergic/Tyraminergic (α-TDC2, magenta), Proctolin (α-Proctolin, yellow), Cholinergic (α-ChAT, cyan) and AllatostatinA (α-AstA, green) immunoreactivity. Arrows point to posterior protocerebral commissure.

Figure 9: A potential central complex in *U. diversus*

(**A.**) 3D renderings of averaged U. diversus synganglion with annotations of potential central complex constituents in shades of green (protocerebral bridge, arcuate body lobes, tonsillar neuropil), also showing the mushroom body (purple) (**B.**) 3D neuropil renderings from of neuropils of the central complex as found in the insects *Rhyparabia maderae*, *Scarabaeus lamarcki*, and *Manduca sexta* (images from insectbraindb.org)

Fig. S1: Cholinergic population expression pattern (α-ChAT immunoreactivity)

α-ChAT (cyan) and α-synapsin (gray) immunoreactivity across the synganglion, top part of image is posterior and bottom is anterior (**A.**) ventral subesophageal ganglion displaying medially located ChAT+ somata of various sizes and staining intensity, as well as somata between leg neuromeres (**B.**) further dorsal slice in the subesophageal ganglion showing abundant staining throughout, arrows mark small intensely ChAT+ somata just ventral to the pedipalpal neuropil (**C.**) overlay with synapsin-immunoreactivity in the subesophageal ganglion (**D.**) anteriorly located cluster of the most intensely ChAT+ somata in proximity to the esophageal passage closure (**E.**) plane dorsal to esophageal closure, with immunoreactivity in the stomodeal bridge, opisthosomal neuropul and protocerebral tract (**F.**) supraesophageal ganglion expression at the plane of the mushroom bodies (**G.**) plane just dorsal to the mushroom body heads, showing putative globuli cells (arrows) within the protrusion of the secondary visual pathway, DAPI stain (red) (**H.**) further dorsal supraesophageal slice, large arrow marks a couple of very large, strongly stained ChAT+ neurons, smaller arrow shows medially located smaller ChAT+ somata, and arrowheads point to string of ChAT+ somata in the posterior cell layer (**I.**) far dorsal end of supraesophageal ganglion showing dispersed ChAT+ somata in the dorsal cap. Arrows indicate arcs of immunoreactivity part of the protocerebral bridge.

Fig. S2: GABAergic population expression pattern (α-GAD immunoreactivity).

α-GAD (red) and α-synapsin (gray) immunoreactivity across the synganglion, top part of image is posterior and bottom is anterior. Lack of signal in interior of tissue is due to poor penetrance of this antibody (**A.**) GAD-immunoreactive somata in the far ventral subesophageal ganglion (**B.**) in a more dorsal plane (**C.**) GAD+ somata ventral to the opisthosomal neuromere (**D.**) GAD-immunoreactivity at the level of the stomodeal bridge, showing ample somata anteriorly, and innervation of the opisthosomal neuropil (**E.**) split views of GAD and synapsin immunoreactivity at the level of mushroom body heads, with arrow indicating a (**F.**) supraesophageal ganglion view at the level of the tonsillar neuropil showing a grouping of GAD+ somata appearing in the medio-lateral axis (**G.**) dorsal supraesophageal ganglion view revealing columns of GAD+ somata on the anterior side as well as

dispersed somata along the arcuate body, immunoreactivity of the protocerebral bridge centrally, and faintly visible neurites crossing perpendicular to the arcuate body layers.

Fig. S3: Dopaminergic population expression pattern (α-TH immunoreactivity).

α-TH (green) immunoreactivity across the synganglion, top part of image is posterior and bottom is anterior (**A.**) TH+ somata in the ventral subesophageal ganglion, with brightened view on right. The approximate boundary of the tissue marked by the dotted line. Each leg neuropil is associated with a cluster of somata made of a smaller, more numerous population (arrowheads), and 1-2 larger neurons (arrows) (**B.**) maximum projection focus on the mesh-like filling of leg neuropils by TH varicosities, dotted line showing perimeter of leg neuropil 2, as an example (**C.**) Fibers of the ventral-most tract travelling parallel to the midline and showing commissures. Arrows mark a cluster of somata ventral to the pedipalpal neuropil which project to the pedipalpal and cheliceral commissures (**D.**) further dorsal view of the subesophageal ganglion, the thicker medial tracts running in the anterio-posterial axis are part of the intermediate-tracts (as defined by Auletta et al., 2019(*4*)), the thinner lateral tract (left side) is part of the ventral-most tract (**E.**) fully visible intermediate-tract, containing a chiasm is seen medially, the ventral tract fibers are lateral and also give rise to 6 major midline crossing commissures, representing the 4 leg neuropils and pedipalpal and cheliceral neuropils. Somata ventral to the opisthosomal neuropil are seen posteriorly (**F.**) Tandem clusters of two pairs of TH+ somata (arrows) adjacent to the closure of the esophageal passage, with immunoreactivity visible in the stomodeal bridge (asterisk) just posteriorly. Arrowhead marks the descending projection of the 4 lateral neurons, presented in the next two subfigures. Opisthosomal neuropil immunoreactivity (brace) shows thick tracts on the perimeter, and crossing fibers internally, as well as somata on the lateral aspect. (**G.**) maximum projection of ventral supraesophageal, arrows marking an additional cluster of 5 TH+ somata, dorsal to the preceeding subfigure. (**H.**) Four neuron lateral cluster (arrow) giving rise to projections joining within the protocerebral dorsal tract as well as a subset descending to the intermediate-tract of the subesophageal ganglion (**I. – J.**) Max projection views of the dorsal supraesophageal ganglion where a single (arrows) and doublet (arrowheads) contribute substantially to the TH immunoreactivity in this region, with the doublet population arching laterally to join the PCDT, and single medial neuron also contributing, while innervating the arcuate body layer seen in (**K.**) where a cluster of 2 or 3 TH+ somata are found centrally, which do not have a counterpart in previously examined species.

Fig. S4: Serotoninergic population expression pattern (α-5-HT immunoreactivity).

α-5-HT (green) and α-synapsin (gray) immunoreactivity across the synganglion, top part of image is posterior and bottom is anterior (**A.**) ventral subesophageal ganglion where clusters of ~5 somata positive for 5-HT are seen at the medial aspect of the leg neuropils (**B.**) further dorsal subesophageal ganglion plane showing pattern of neuropil innervation (brace) comprised of a posterior and anterior half, leaving a dearth of signal in the center of the neuropil (**C.**) 5-HT+ somata present anteriorly (arrows), ventral to the pedipalpal neuropil, pathways of the ventral-tract appear internally (**D.**) 5-HT immunoreactive somata (arrows) with thick neurites found ventral to the opisthosomal neuropil (**E.**) beginning planes of the supraesophageal ganglion showing a bridging commissure on the posterior side, with pronounced immunoreactivity in the adjacent region (**F.**) multiple strong 5-HT+ puncta adjoin the

1424 protocerebral tract synapsin densities suggesting 5-HT fibers are a part of this tract. A distinctive circular
1425 structure forms (**G.**) through arches of innervation travelling medially to midline varicosities (**H.**) which
1426 all intersect, beginning innervation just anteriorly of the hagstone neuropil. In the posterior
1427 supraesophageal ganglion at this plane an umbrella-like structure of fine varicosities appears (**I.**)
1428 Continuation of the umbrella-like structure found posteriorly, with expanding immunoreactivity in the
1429 hagstone neuropil (brace) found aside the midline (**J.**) strongly immunoreactive 5-HT neurons near the
1430 plan of the mushroom body head, whose neurites innervate the area found laterally to the somata. (**K.**)
1431 faint evidence of 5-HT+ populations in the far dorsal supraesophageal ganglion, 5-HT immunoreactivity
1432 in layers of arcuate body seen posteriorly.

1433

1434 **Fig. S5: Octopaminergic/Tyraminergic population expression pattern (α-TDC2 immunoreactivity).**

1435 α-TDC2 (magenta) and α-synapsin (gray) immunoreactivity across the synganglion, top part of image is
1436 posterior and bottom is anterior (**A.**) ventral subesophageal ganglion horizontal optical slice showing
1437 medial clusters of TDC2+ somata corresponding to each leg neuropil (**B.**) maximum intensity projection
1438 of ventral subesophageal ganglion demonstrating an anterior/posterior division in innervation pattern
1439 within each leg neuropil, with sparse heavy puncta posteriorly and denser but diffuse patterning
1440 anteriorly (**C.**) Bright TDC2+ somata (arrows) ventral to the opisthosomal neuropil, TDC2+
1441 immunoreactivity in the medial fiber tracts and pedipalpal neuropil (**D.**) horizontal optical slice showing
1442 opisthosomal neuromere posteriorly, and anteriorly the region ventral to the closure of the esophageal
1443 passage. Anteriolaterally, TDC2+ immunoreactivity is seen in the cheliceral neuropil. A triangular
1444 strucuture (brace) is formed as strings of puncta travel posteriorly to become heavier on the lateral
1445 perimeters of the opisthosomal neuropil. Interiorly there is a ring-like structure and chiasm with fine
1446 spoke neurites connecting to it (**E.**) the same view as preceeding but overlayed onto α-synapsin
1447 immunoreactivity (**F.**) maximum intensity projection encompassing a span from the level of the
1448 esophageal passage to the appearance of the bridge, where a cluster of 15-20 TDC2+ somata are found
1449 (arrows). The opisthosmal neuropil displays strings of immunoreactivity along the borders, roughly
1450 parallel to the midline, as well as travelling laterally across the halves of the neuropil (**G.**) TDC2+
1451 immunoreactivity is present in the stomodeal bridge, seen immediately posterior to the somata clusters.
1452 In the opisthosomal neuropil, pronounced tracts run along the length of the midline, with a fine arching
1453 commissure at the posterior end (arrow). (**H.**) maximum intensity projection of planes just dorsal to the
1454 preceeding figure demonstrate a lateral nested pathway of longitudinal puncta, and an additional strand
1455 positioned in the medial-lateral direction (brace) (**I.**) supraesophageal ganglion plane at the level of the
1456 MB hafts displays ample TDC2+ immunoreactivity, with presence in the umbrella-like structure at the
1457 posterior side, sparser puncta within the bounds of the hagstone neuropil, and signal found anterio-
1458 medially to the mushroom body (**J.**) which continues in these areas dorsally to the level of the
1459 mushroom body heads, where strands of immunoreactivity also follow the contours of the lateral edges
1460 of the supraesophageal ganglion (**K.**) α -TDC2 (magenta) and α -5-HT (green) immunoreactivity overlaps
1461 in the centrally located tonsillar neuropil, showing TDC2+ signal in a peripheral pattern, with more 5-HT+
1462 immunoreactivity at the center of the neuropil. (**L.**) subesophageal ganglion plane at the level of the
1463 arcuate body and protocerebral bridge, with magnification focusing on a series of puncta (arrows) which
1464 might be indicative of innervation to or passage by the tonsillar neuropil (**M.**) Further dorsal maximum
1465 intensity projection from supraesophageal ganglion, with TDC2+ somata (arrow), and innervation
1466 patterns of the ventral and dorsal arcuate body lobes visible posteriorly.

1467

1468 **Fig. S6: AllatostatinA population expression pattern (α-AstA immunoreactivity).**

1469 α-AstA (green) and α-synapsin (gray) immunoreactivity across the synganglion, top part of image is
1470 posterior and bottom is anterior (**A.**) ventral subesophageal ganglion slice with clusters (arrow) and
1471 individual AstA+ somata (**B.**) maximum intensity projection of planes in the subesophageal ganglion
1472 revealing AstA+ varicosities in the posterior halves of the leg neuropils (**C.**) AstA+ immunoreactivity in
1473 lateral branches of the centro-lateral tract, supplying the leg neuropils (**D.**) a section of AstA+
1474 immunoreactivity is visible adjacent to the esophagus (brace) with (**E.**) thin neurites at the crossing of
1475 the stomodeal bridge (arrow). Paired longitudinal strands of puncta are seen extending into the
1476 opisthosomal neuromere, posteriorly (**F.**) a more robust commissure and appreciable immunoreactivity
1477 is seen on the posterior side of the ventral supraesophageal ganglion (**G.**) Medially-arching circular
1478 pattern of AstA+ immunoreactivity in the posterior supraesophageal ganglion, similar to 5-HT signal in
1479 the same region (**H.**) Plane of supraesophageal ganglion at the level of the mushroom body hafts,
1480 showing strong expression on the posterior side, AstA+ immunoreactivity encompassing the umbrella-
1481 like form seen in other stains (5-HT, TDC2). A cluster of ~7 AstA+ somata are visible in the anterior field
1482 (arrows) (**I.**) a pair of large, intensely AstA+ somata are present deep within the furrow of the anterior
1483 somata field, sending neurites into the immediately posterior tonsillar neuropil, whose shape is
1484 distinguishable (**J.**) Just dorsally, the centrally located tonsillar neuropil is still visible, as the arching
1485 posterior protocerebral commissure is visible laterally and posteriorly. A pair of AstA+ somata are
1486 present laterally. (**K.**) AstA+ innervation of the posterior side of the ventral arcuate body (ABv), with
1487 circular units of immunoreactivity visible on the posterior edge (arrowheads), suggestive of columnar
1488 structure.

1489

1490 **Fig. S7: Proctolin population expression pattern (α-Proctolin immunoreactivity).**

1491 α-Proctolin (yellow) and α-synapsin (gray) immunoreactivity across the synganglion, top part of image is
1492 posterior and bottom is anterior (**A.**) maximum intensity projection of ventral subesophageal ganglion
1493 showing a single brightly Proctolin+ neuronal cell body per each leg neuropil. More faintly labelled
1494 Proctolin+ somata are also visible (**B.**) Optical plane in the subesophageal ganglion at the level of the
1495 pedipalpal neuropil, showing a cluster of Proctolin+ somata (arrow) and a concentration of signal in the
1496 immediately posterior-medial vicinity. Small Proctolin+ somata are also seen in the field ventral to the
1497 opisthosomal neuropil (arrowheads). (**C.**) further dorsal view of the subesophageal ganglion at the level
1498 of commissures of the major dorsal tract. Densely-immunoreactive pair of roughly circular shapes
1499 (arrow) represent a tract which is rising directly dorsally (**D.**) Proctolin+ immunoreactivity is present in
1500 the opisthosomal neuropil, covering similar trajectories as other immunostains (e.g. TDC2), but in a
1501 more fragmentary manner (**E.**) Optical section at the level of the stomodeal bridge, featuring Proctolin
1502 immunoreactivity crossing the midline on the anterior and posterior bounds of the bridge. Proctolin
1503 immunoreactivty is also seen concentrated adjacent to the midline on the posterior side of the emerging
1504 supraesophageal ganglion, which is seen further dorsally (**F.**) in addition to immunoreactivity in a patch
1505 medial to the synapsin-negative channel through which the protocerebral tract travels, a zone not
1506 obviously present with other immunostains. (**G.**) Proctolin+ somata become visible in the anterior
1507 somata field beginning at the level of the mushroom body hafts, where Proctolin immunoreactivity is
1508 concentrated posteriorly about the midline, and the hagstone neuropil is also highlighted. (**H.**) Further

1509 dorsally as the mushroom body develops, crescents of Proctolin immunoreactivity are nested within the
1510 cup-shape structure formed by the mushroom body hafts and body, which is also a distinctive feature of
1511 α-Proctolin staining. Somata continue in the anterior furrow, likewise (**I.**) further dorsally where faint
1512 Proctolin+ somata (arrow) are present at the level of the mushroom body heads (**J.**) At this level too, as
1513 shown in a maximum intensity projection of the neighboring planes, a strongly immunoreactive strand
1514 of varicosities begins anterio-laterally (brace) (**K.**) continuing posterior-medially, to bifurcate into a
1515 medial and posterior facing branch (brace). Proctolin immunoreactivity is seen centrally in the posterior
1516 aspect of the tonsillar neuropil. (**L.**) maximum intensity projection spanning planes in the previous
1517 subfigure as well as dorsal ones overlays a dorsal strand of immunoreactivity which we describe as a
1518 dorsal posterior protocerebral commissure, crossing the midline just anterior to the arcuate body (**M.**)
1519 maximum intensity projection of planes of far dorsal supraesophageal ganglion showing Proctolin+
1520 somata distributed centrally and laterally, layering pattern of the ventral and dorsal arcuate body lobes
1521 is also visible posteriorly.

1522

1523 **Fig. S8: Crustacean cardioactive peptide population expression pattern (α-CCAP immunoreactivity).**

1524 α-CCAP (red) and α-synapsin (gray) immunoreactivity across the synganglion, top part of image is
1525 posterior and bottom is anterior (**A.**) maximum intensity projection of ventral supraesophageal ganglion
1526 showing clustering of CCAP+ somata (**B.**) further dorsal plane showing sparsely located CCAP+ somata,
1527 as well as the immunoreactivity pattern within the leg neuropils made of a evenly-spaced distribution of
1528 bright puncta but only in the posterior portion of each neuropil (**C.**) CCAP immunoreactivity is visible
1529 anteriorly around the pedipalpal neuropil, and faint CCAP+ somata are also seen in the area ventral to
1530 the opisthosomal neuropil (arrow). (**D.**) Horizontal optical slice at the plane of the stomodeal bridge
1531 showing where CCAP immunoreactivity is present. Dense staining is also apparent in the opisthosomal
1532 neuropil (**E.**) Supraesophageal ganglion plane at the level of the mushroom bodies where CCAP
1533 immunoreactivity is punctate broadly across the tissue, with some concentrations in the posterior
1534 umbrella-like structure and the anterior bounds of the hagstone neuropil (**F.**) Supraesophageal ganglion
1535 plane at the emergence of the ventral arcuate body lobe, with arrow marking the ventral trajectory of
1536 the PCDt (**G.**) maximum intensity projection of planes in the vicinity of the ventral arcuate body lobe,
1537 showing clustering of CCAP+ somata deep and medial in the anterior furrow of neuronal cell bodies (**H.**)
1538 dispersed CCAP+ somata at the dorsal end of the supraesophageal ganglion, with abundant CCAP
1539 innervation of all layers of the arcuate body seen posteriorly.

1540

1541 **Fig. S9: FMRFamide population expression pattern (α-FMRFamide immunoreactivity).**

1542 α-FMRFamide (red) and α-synapsin (gray) immunoreactivity across the synganglion, top part of image is
1543 posterior and bottom is anterior (**A.**) ventral subesophageal ganglion showing distribution of
1544 FMRFamide+ somata (**B.**) FMRFamide immunoreactivity in the leg neuropils and somata present among
1545 the cell bodies ventral to the opisthosomal neuropil (arrows) (**C.**) a dorsal subesophageal plane at the
1546 level of the major neuropil commissures showing FMRFamide immunoreactivity (**D.**) FMRFamide+
1547 somata in the anterior cell body wall (arrows), with immunoreactivity around the cheliceral neuropil.
1548 FMRFamide innervation of the opisthosomal neuropil is also apparent (**E.**) continuing dorsally, at the
1549 plane of the stomodeal bridge (**F.**) FMRFamide immunoreactivity is extensive across the

supraesophageal ganglion, as seen for the plane of the mushroom body (**G.**) as well as further dorsally where the arcuate body emerges. An approximately rectangular pattern of immunoreactivity (brace) is seen posterior to the tonsillar neuropil, which is distinctive to FMRFamide immunoreactivty. FMRFamide signal is seen posteriorly in both sublayers of the ventral arcuate body (**H.**) while a pronounced layer of FMRFamide immunoreactivity appears in the posterior aspect of the dorsal arcuate body layer. FMRFamide+ somata are abundantly distributed across the dorsal end of the supraesophageal ganglion.

Figure 1

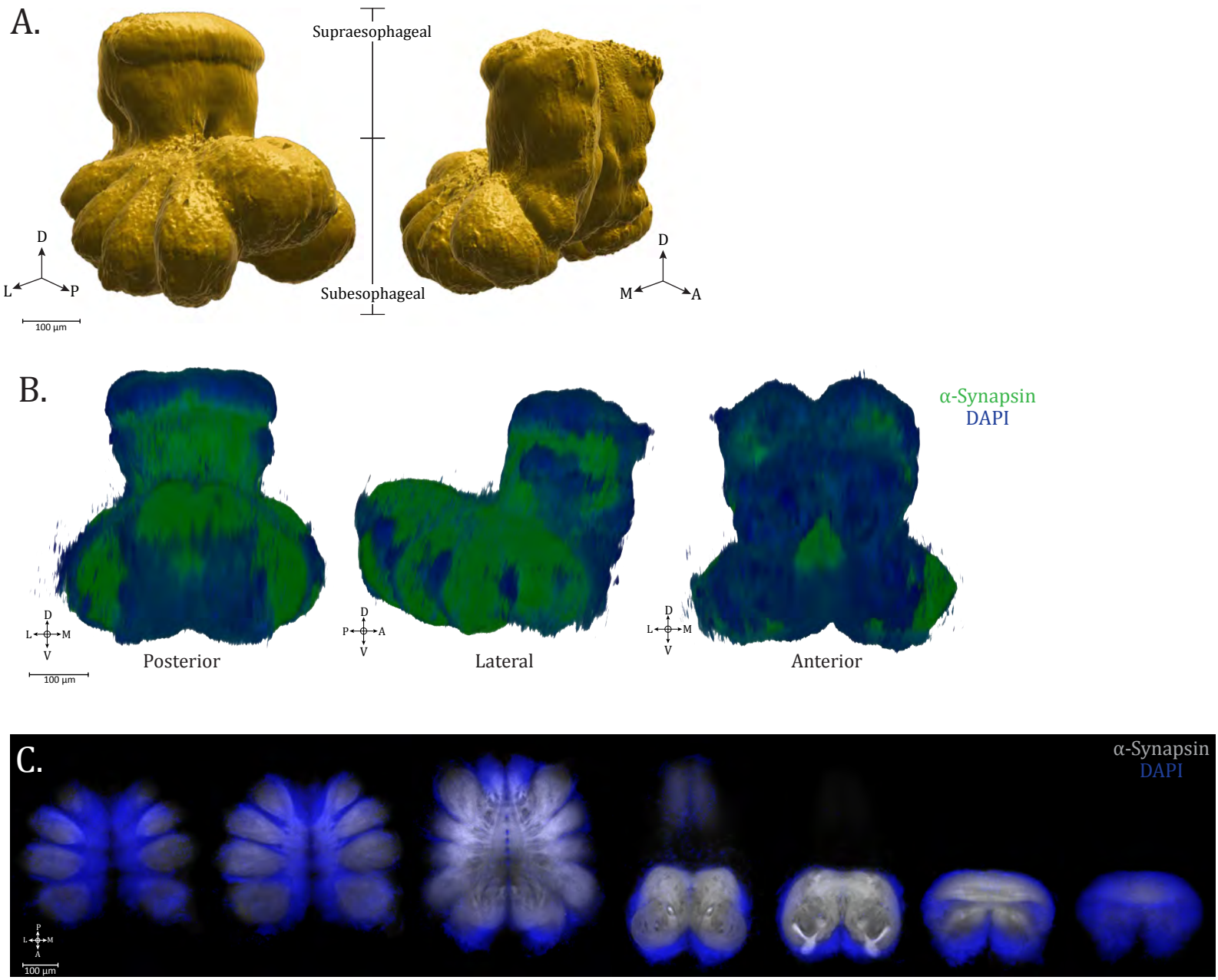
A.
Supraesophageal
Subesophageal
D
L
P
M
A
100 µm
B.
α-Synapsin
DAPI
Posterior
Lateral
Anterior
100 µm
C.
α-Synapsin
DAPI
100 µm

Figure 2

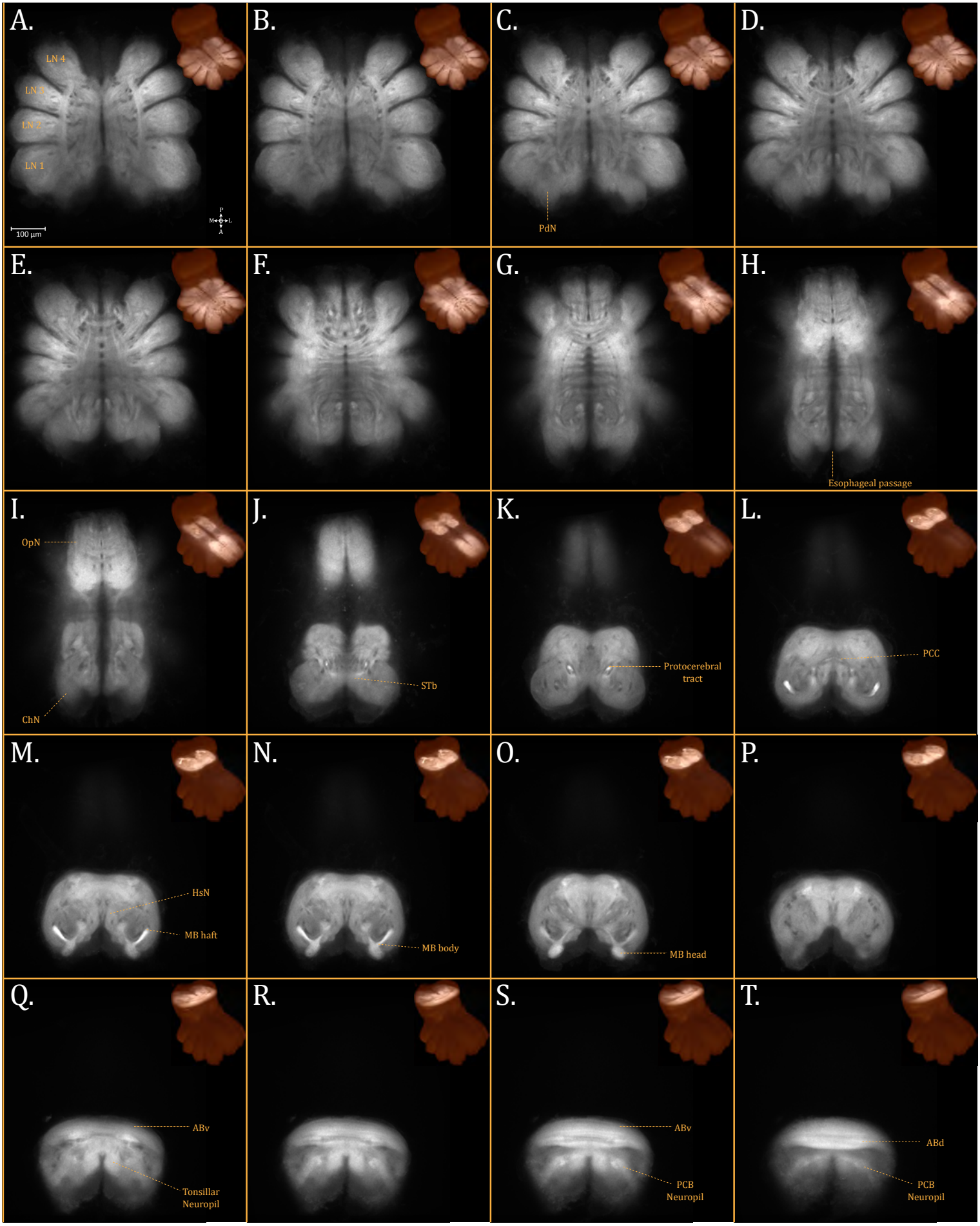
A.
LN 4
LN 3
LN 2
LN 1
100 µm
P
M
L
A
B.
C.
PdN
D.
E.
F.
G.
H.
Esophageal passage
I.
OpN
ChN
J.
STb
K.
Protocerebral tract
L.
PCC
M.
HsN
MB haft
N.
MB body
O.
MB head
P.
Q.
ABv
Tonsillar Neuropil
R.
S.
ABv
PCB Neuropil
T.
ABd
PCB Neuropil

Figure 3

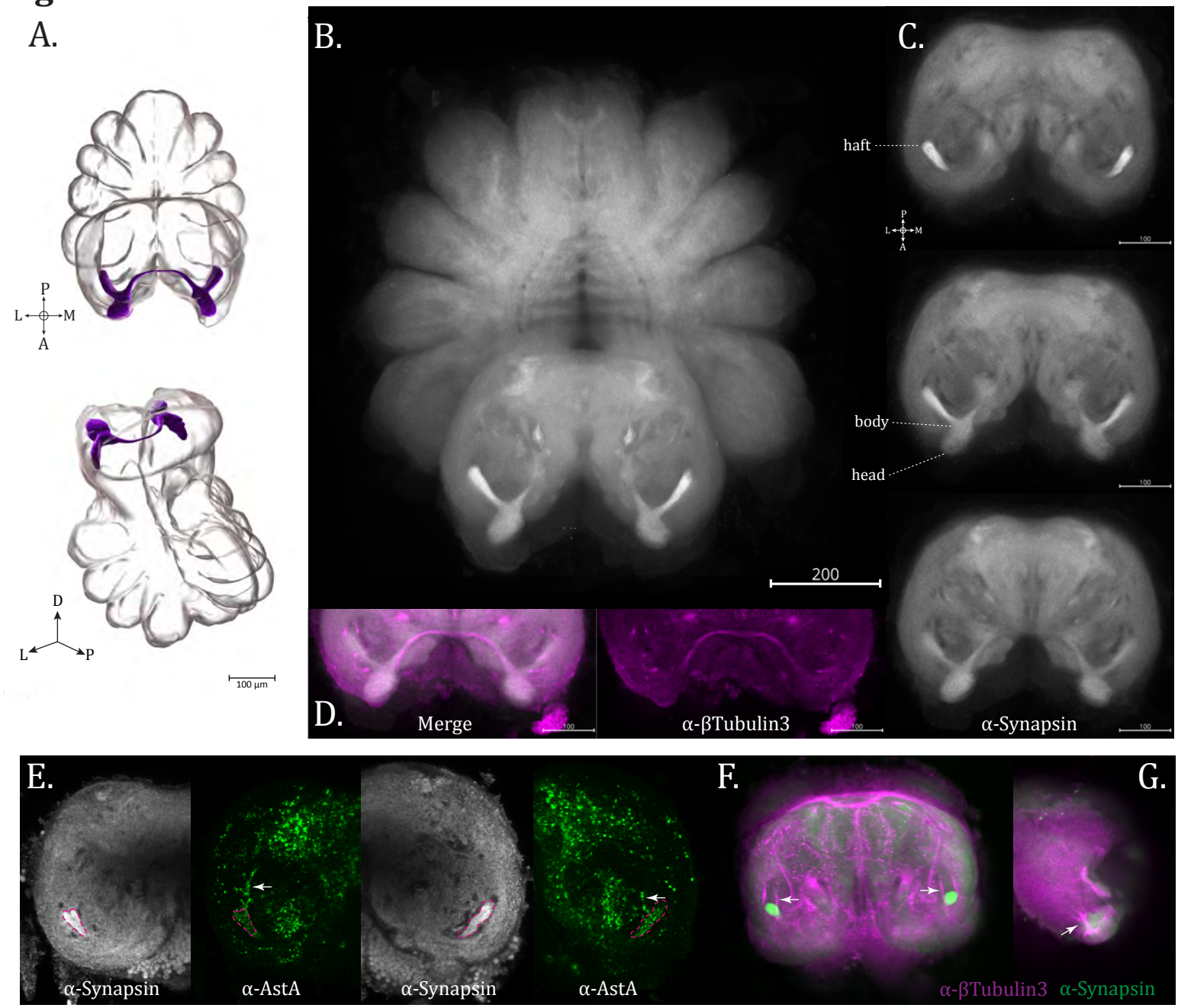
A.
P
L
M
A
D
L
P
100 µm
B.
200
C.
haft
P
L
M
A
body
head
D.
Merge
α-βTubulin3
α-Synapsin
E.
α-Synapsin
α-AstA
α-Synapsin
α-AstA
F.
α-βTubulin3
α-Synapsin
G.

Figure 4

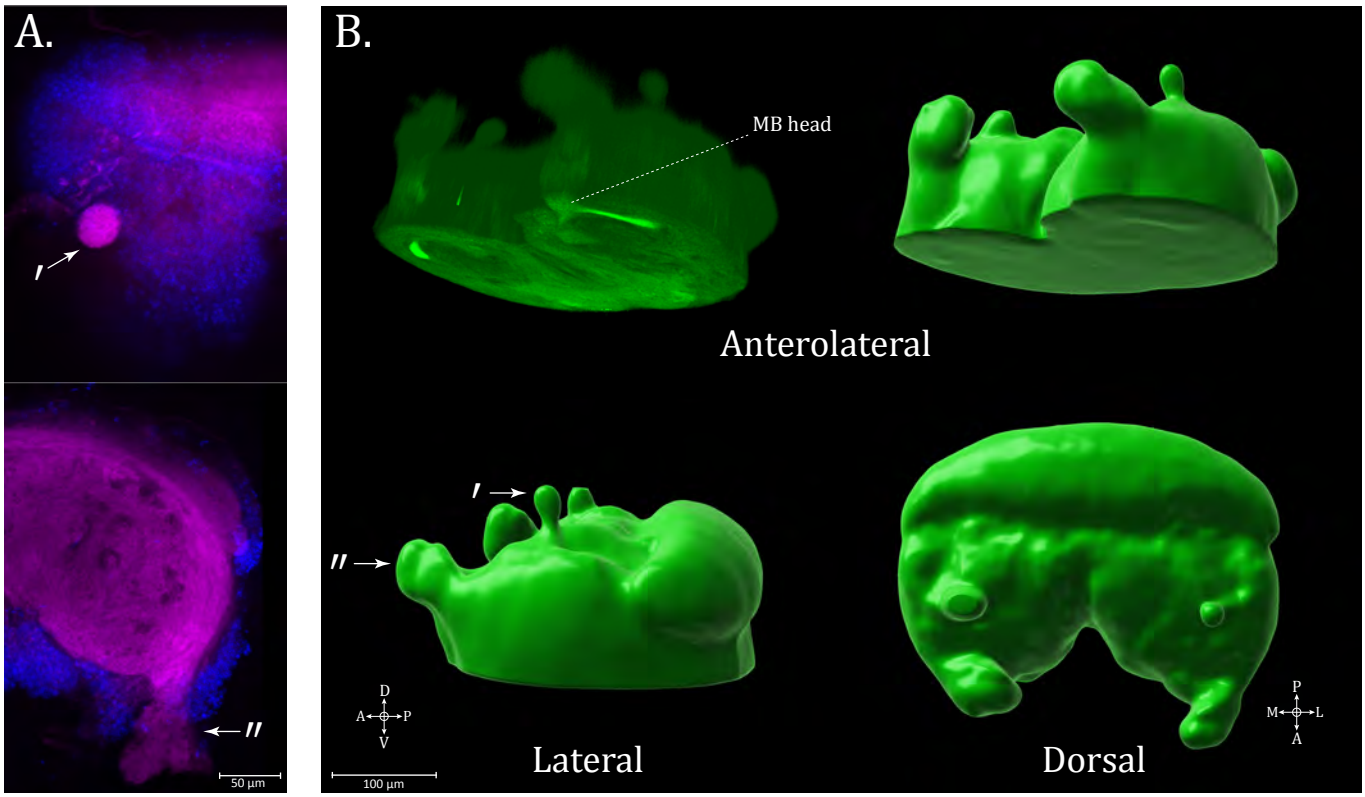
A.
I
II
50 µm
B.
MB head
Anterolateral
I
II
D
A
P
V
100 µm
Lateral
P
M
L
A
Dorsal

Figure 5

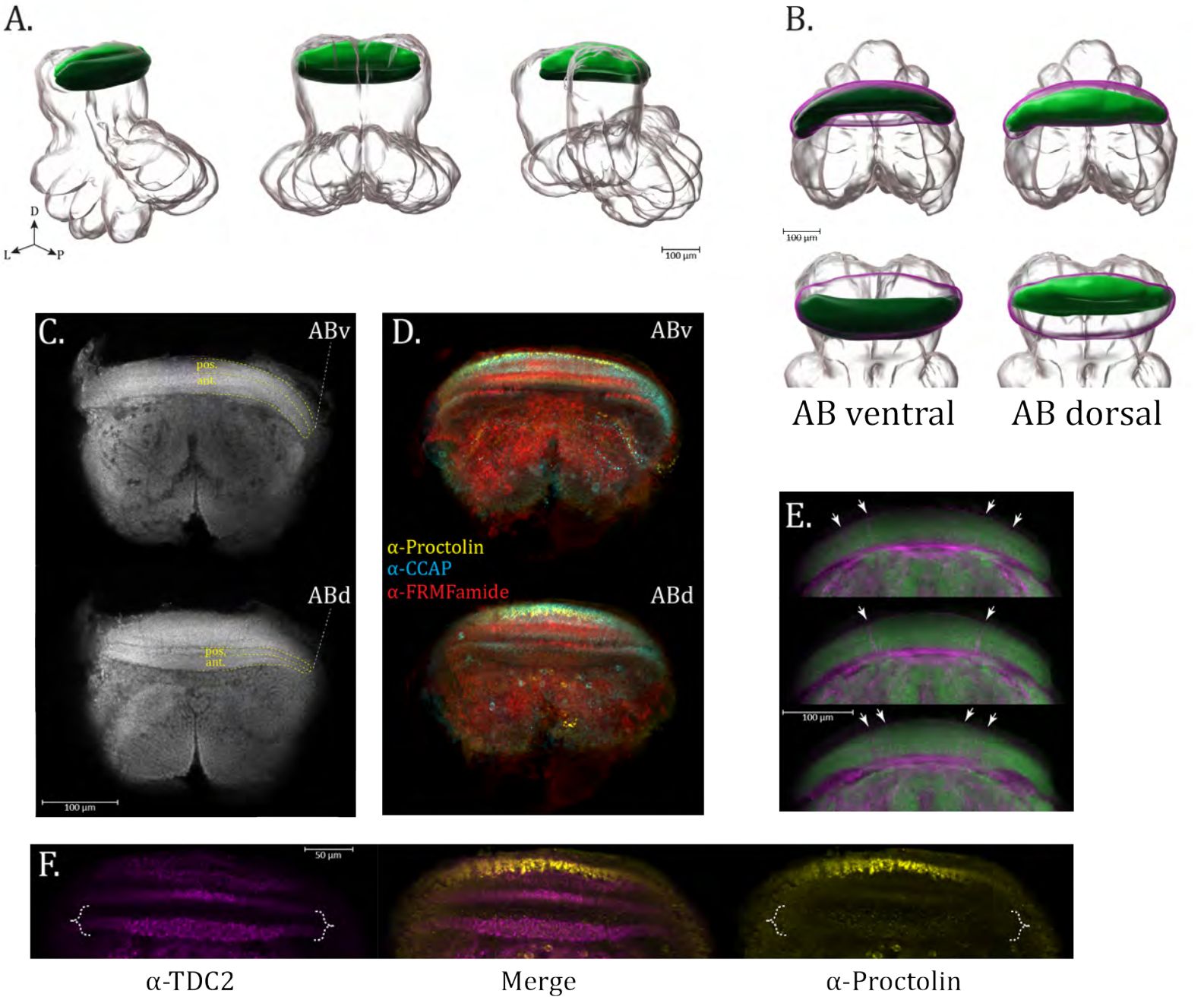
A.
D
L
P
100 µm
B.
100 µm
AB ventral
AB dorsal
C.
ABv
pos.
ant.
ABd
pos.
ant.
100 µm
D.
ABv
α-Proctolin
α-CCAP
α-FRMFamide
ABd
E.
100 µm
F.
50 µm
α-TDC2
Merge
α-Proctolin

Figure 6

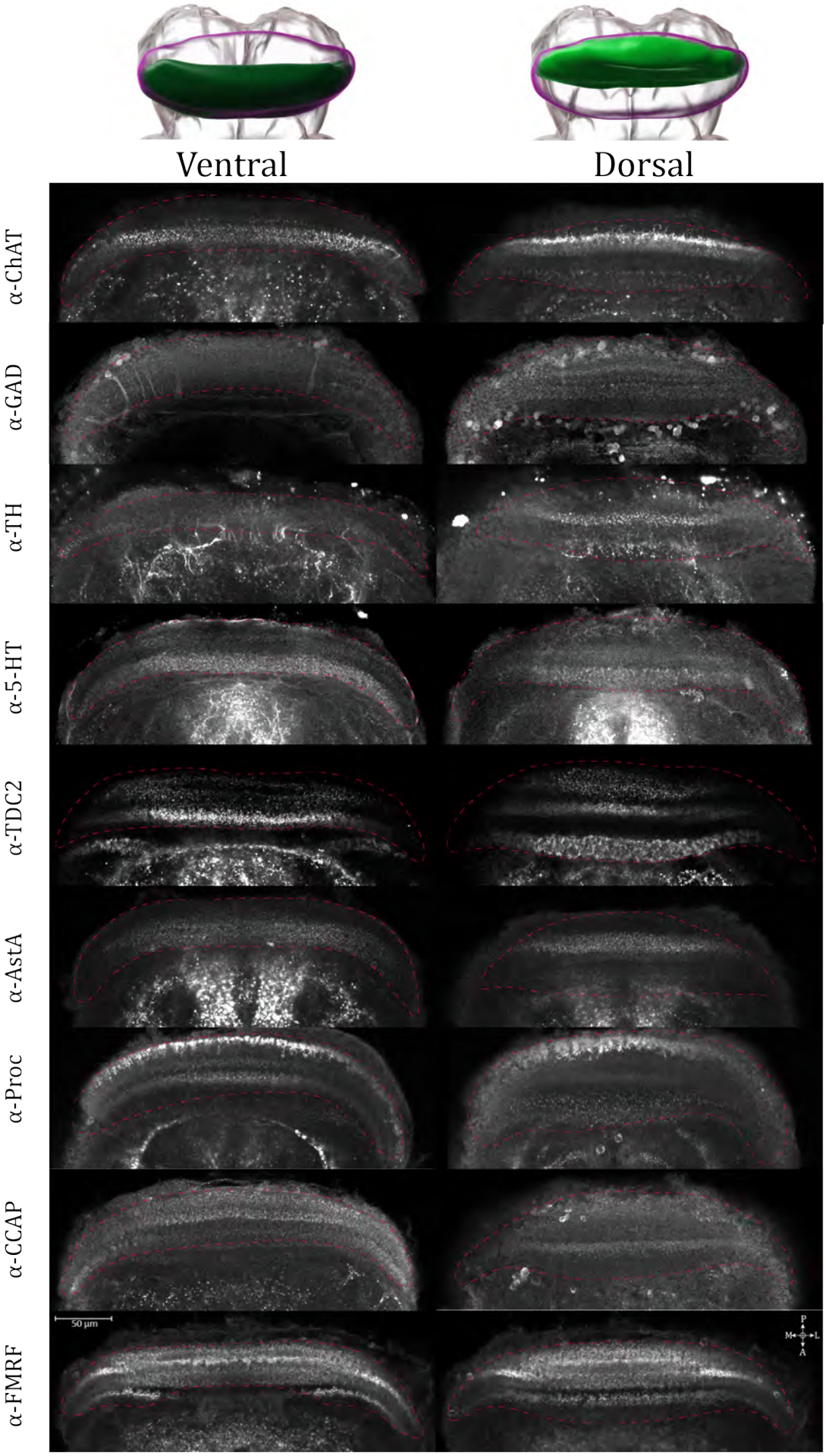
Ventral
Dorsal
α-ChAT
α-GAD
α-TH
α-5-HT
α-TDC2
α-AstA
α-Proc
α-CCAP
α-FMRF
50 µm
P
M
L
A

Figure 7

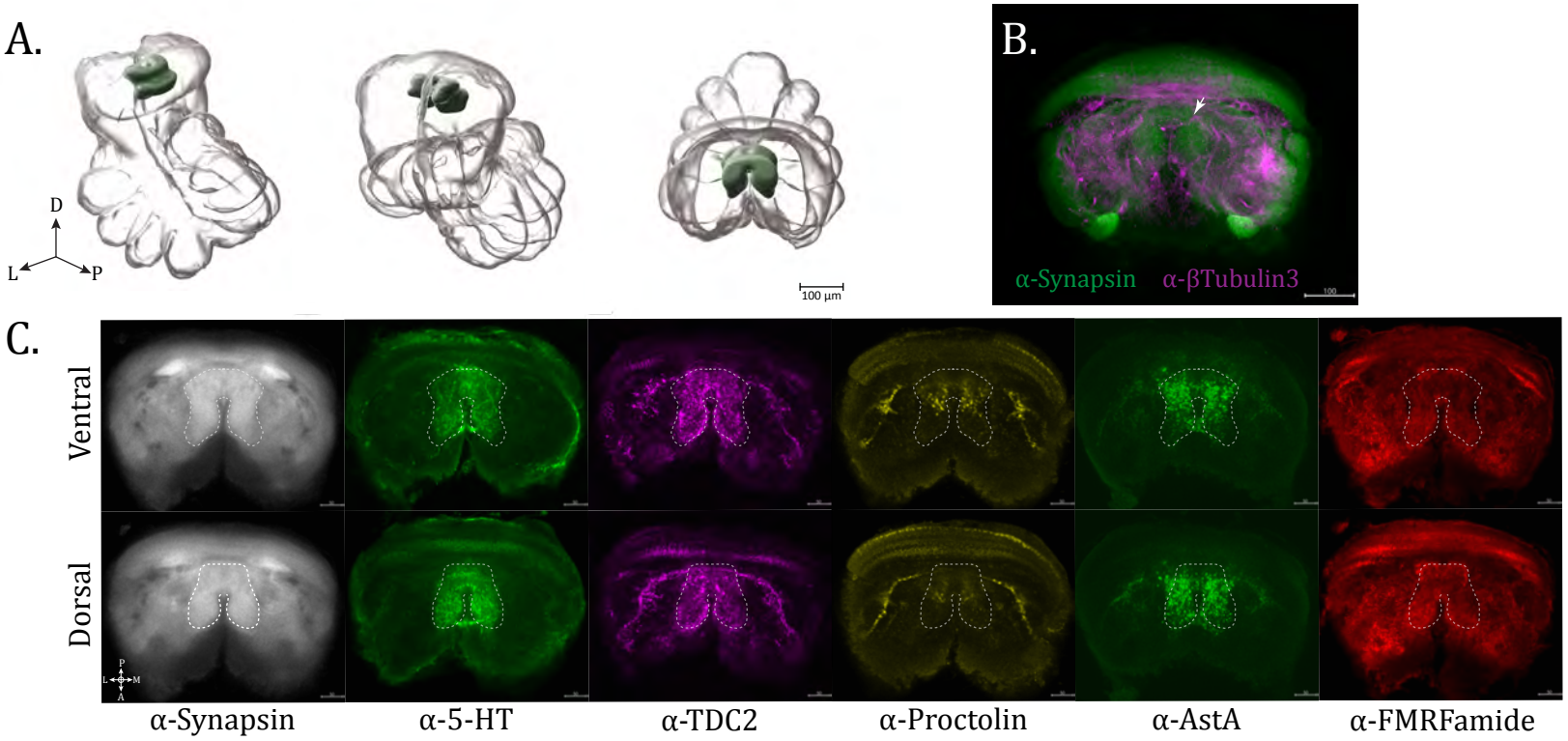
A.
D
L
P
100 µm
B.
α-Synapsin
α-βTubulin3
C.
Ventral
Dorsal
α-Synapsin
α-5-HT
α-TDC2
α-Proctolin
α-AstA
α-FMRFamide

Figure 8

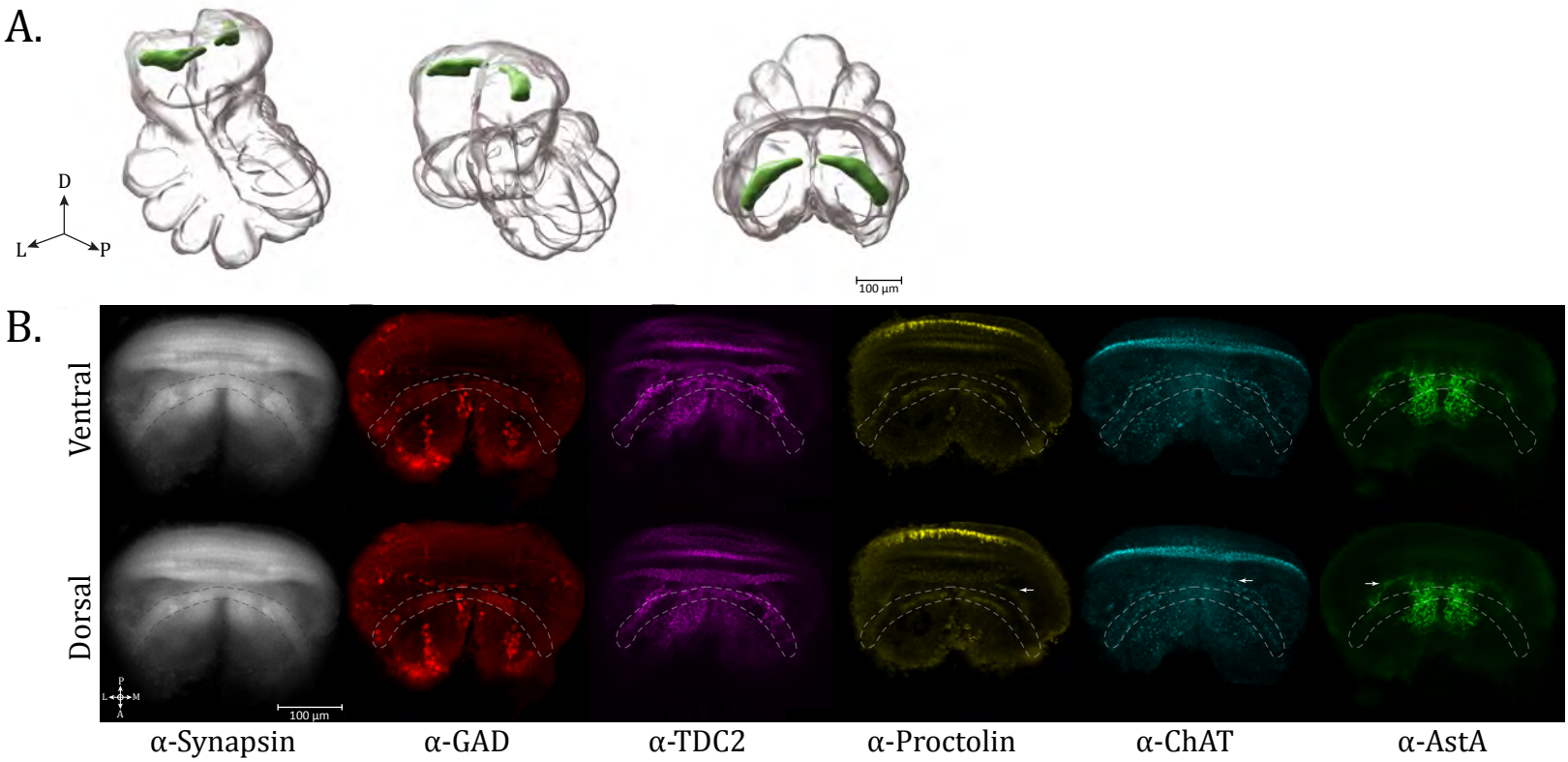
A.
D
L
P
100 µm
B.
Ventral
Dorsal
P
L
M
A
100 µm
α-Synapsin
α-GAD
α-TDC2
α-Proctolin
α-ChAT
α-AstA

Figure 9

A.

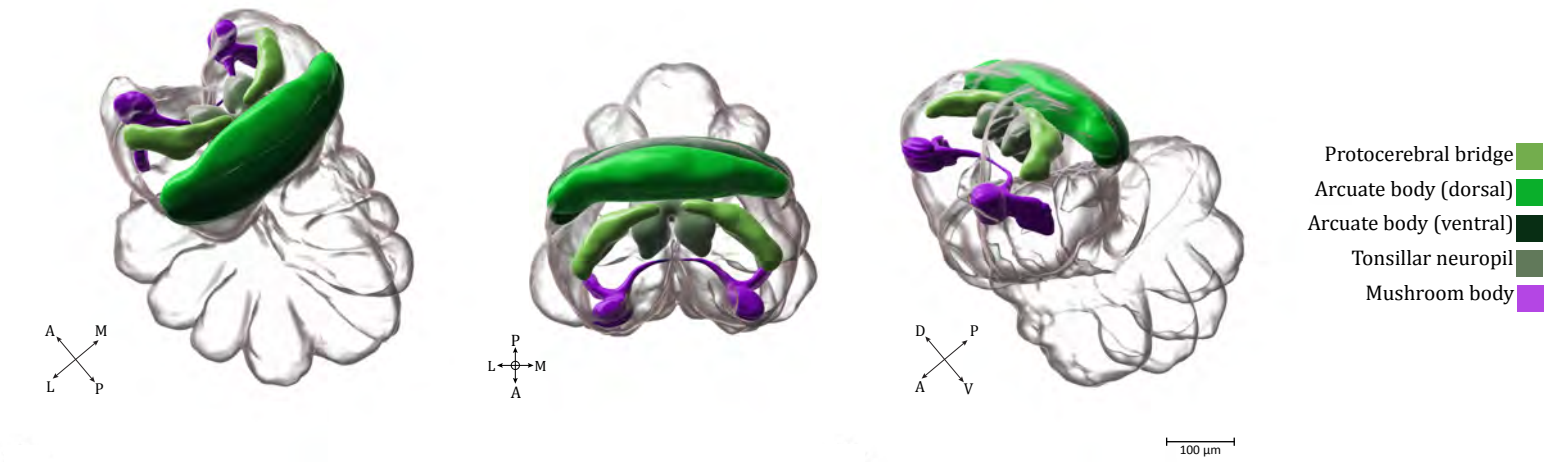

B.

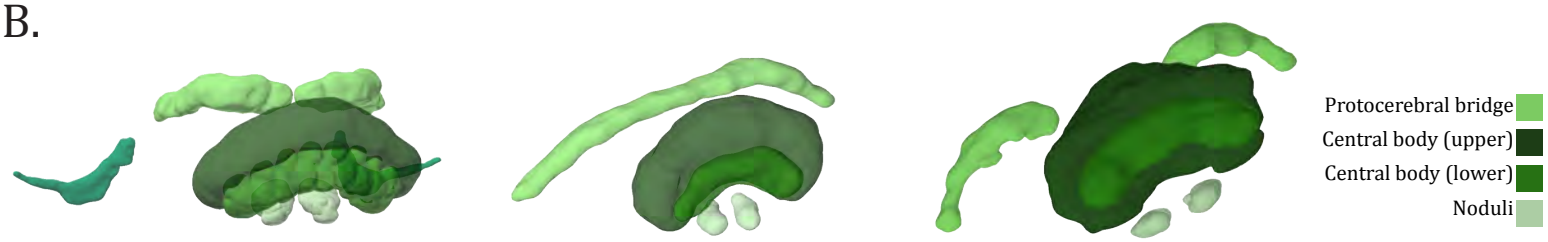

Rhyparabia maderae
(Cockroach)

Scarabaeus lamarcki
(Scarab beetle)

Manduca sexta
(Moth)

insectbraindb.org